

## Review

# High-valent first-row transition-metal complexes of tetraamido (4N) and diamidodialkoxido or diamidophenolato (2N/2O) ligands: Synthesis, structure, and magnetochemistry

Delia-Laura Popescu, Arani Chanda, Matthew Stadler, Filipe Tiago de Oliveira, Alexander D. Ryabov, Eckard Münck, Emile L. Bominaar<sup>\*</sup>, Terrence J. Collins<sup>\*</sup>

*Department of Chemistry, Carnegie Mellon University, 4400 Fifth Avenue, Pittsburgh, PA 15213, USA*

Received 25 July 2007; accepted 7 November 2007

Available online 17 November 2007

## Contents

1. Introduction .....	2051
2. A ligand survey .....	2052
3. High-valent mononuclear complexes .....	2054
3.1. Manganese complexes .....	2054
3.2. Cobalt complexes .....	2056
3.3. Chromium, nickel, and copper complexes .....	2058
3.3.1. Chromium complexes .....	2058
3.3.2. Nickel complexes .....	2059
3.3.3. Copper complexes .....	2059
3.4. On TAML innocence in M[MAC*] complexes .....	2060
3.5. What do the DFT results mean for the oxidation state assignment at the metal and the related concept of the innocence of $[Q^1]^{4-}$ ? .....	2060
3.6. What do the DFT results mean for the broader understanding of the electronic structures of $MQ^1$ systems and for the interpretation of spectroscopic properties? .....	2062
3.7. What might the DFT results mean for the reaction chemistry of $MQ^1$ complexes? .....	2063
4. Magnetochemistry .....	2064
5. Conclusions .....	2069
References .....	2070

## Abstract

Introduced approximately two decades ago, macrocyclic deprotonated tetraamido (4N) and, nearly a decade earlier, acyclic diamidodialkoxido or diamidophenolato (2N/2O) ligand systems have been used, among other things, for the synthesis of a wide variety of high-valent complexes of iron, manganese, cobalt, vanadium, nickel, chromium, and copper. Structural, magnetic, and catalytic properties of these mononuclear, dinuclear, and polynuclear complexes created by the Collins group are reviewed. The present account continues an overview of complexes of this type published recently and devoted to iron species exclusively [Chanda et al., *J. Inorg. Biochem.*, 100 (2006) 606], which provide the first highly effective small molecule mimics of peroxidase enzymes, called TAML activators. The story of the reviewed first-row complexes does not include the diverse and instructive chemistry discovered for osmium, but like the osmium chemistry, it derives its greatest significance from the fact that key members of the various species mark the steps along the design pathway that led to iron-TAML activators. Consideration is given to recent questioning in the literature of the innocence of a TAML system that was designed to be innocent. The reasons underlying the now 15-year old refocusing of our research program on oxidation catalysis and green chemistry with the associated termination of research into designed molecule-based magnetic

<sup>\*</sup> Corresponding authors. Tel.: +1 412 268 6335; fax: +1 412 268 1061.  
E-mail address: [tc1u@andrew.cmu.edu](mailto:tc1u@andrew.cmu.edu) (T.J. Collins).

materials are explained. Our closing contributions from the mid-1990s to the design of molecule-based magnetic materials are reviewed. Previously reported data are discussed in conjunction with newly obtained information on the complexes using density functional theory.

© 2007 Elsevier B.V. All rights reserved.

**Keywords:** High-valent transition metal complexes; TAML complexes; Tetraamido macrocyclic ligand complexes; Diamidodialkoxido complexes; Diamidodiphenolato complexes; Ligand innocence; Molecule-based magnetic materials; Magnetochemistry; Green chemistry

## 1. Introduction

The powerful biological oxidizing systems of peroxidases, cytochrome P450s and similar enzymes [1,2] challenge chemists to understand and to reproduce their exceptional reactivity in synthetic mimics in related or tangential design spaces [3]. The phenomenal oxidizing power of the enzymes coexists with appreciable resistance to “self-oxidation”. This coexistence is achieved by the employment of design elements that direct the selectivity of the reactive intermediates toward rapid substrate oxidation, thus allowing oxidatively fragile components of the enzyme to be kinetically camouflaged and enabling the enzymes to perform numerous catalytic turnovers before they finally succumb to degradation under the intense reactivity pressure. Ideally, synthetic low-molecular-weight catalysts should possess similar functional properties, preferably with an easily accessible range of reactivity, diverse controllable selectivity, and even superior performance especially in terms of the turnover numbers. Now knowing what is needed, we can assert that to create such catalysts requires one to focus intently upon the design and synthesis of appropriate ligand systems that both convey what one imagines will be the required electronic structure to the chosen catalytic metal atom while also being resistant to hydrolysis (given that the most important solvent to master is water) as well as to the aggressive oxidizing conditions that the catalysts are being designed to unleash. Then, after complexation of a suitable metal, the man-made catalyst should activate the primary oxidizing agents of nature, *viz.* hydrogen peroxide and dioxygen. Their oxidizing equivalents should be delivered to target molecules avoiding rapid catalyst self-oxidation of both the suicidal and homicidal varieties.

The Collins group initiated such a design program more than 25 years ago with a focus on learning how to slow down the degradation processes of ligand systems conceived to be electronically capable of supporting appropriate reactive intermediates. This was seen as an alternative and more viable technological approach to the ingenuity in enzyme evolution, which focuses on speeding up the targeted reactions [3]. In recent years, we have been able to confirm that the Collins iterative design protocol, developed to understand how to protect ligand systems from rapid oxidative and hydrolytic degradation, is a *sine qua non* for achieving useful small molecule enzyme-like synthetic catalysts for oxidative processes [4]. At the top of our research pyramid stand iron(III) complexes of the TetraAmido Macrocyclic Ligand (TAML) system [5,6]. These phenomenal activators of hydrogen peroxide in water [3,7,8] and, less usefully at present of dioxygen in weakly coordinating non-aqueous media [9], show superior activity in a variety of industrially, environmentally, and strategically important

processes including persistent pollutant remediation, pulp and paper bleaching [10], chemical effluent treatment, chemical warfare and biological decontamination [11], degradation of persistent chlorinated pollutants [12], desulfurization of diesel fuel [13], fine chemical synthesis, and water purification [14].

A number of TAML systems that deliver the desired catalytic activity have been designed, synthesized and thoroughly explored. But the PolyAnionic Chelating (PAC) ligands that were initially introduced differ noticeably from the more recent TAML systems [15]. Almost a dozen transition metals have been incorporated into PAC ligand and TAML systems. Although only iron-TAML complexes have proven to date to be powerful oxidation catalysts, manganese-TAMLs give less useful catalysts. In addition, the many different metal systems have revealed a spectrum of new features related to general aspects of coordination chemistry showing unusual geometries and coordination numbers, and magnetic properties.

This last area deserves special mention in the introduction, because our having to abandon it was especially chagrining. A design program, complementary to the catalyst design program, was aimed at contributing to developing the synthetic and related thinking required for building magnetic crystals of predetermined magnetic behavior and it was beginning to bear fruit by the early 1990s. This program arose as the unusual higher spin ground states were being found for mononuclear  $M_a$  PAC ligand complexes and it was realized that  $M_a$  PAC species could be coupled to other paramagnetic ions ( $M_b$ ) at the  $M_a(OR)_2$  moieties giving  $M_a(\mu-OR)_2M_b$  multimetallic ions that had the potential to have ground state electronic configurations with high numbers of weakly coupled spins. Moreover, it was realized that high-spin ground states were to be reasonably expected in these multinuclear ions because the unpaired spin structures on  $M_a$  ions are such that they should favor ferromagnetic exchange interactions with  $M_b$  ions whenever  $M_a$  had a d-electron count  $\leq 7$ , regardless of the electronic structure of  $M_b$ . This notion was based on the realization that the principal  $d\sigma$  orbital on  $M_a$  is made especially antibonding by the strong PAC ligand  $\sigma$ -donor system and it was this feature that was giving rise to the high-spin ground states of  $M_a$  PAC species with the d-electrons being distributed among the four remaining more closely grouped d orbitals. Thus, the major  $M_a$  d-orbital communicating through the  $-OR$  bridges with  $M_b$  could reliably be expected to be empty and therefore to interact with  $M_b$  to give ferromagnetic exchange. This, it was further rationalized, meant that the PAC ligand systems offered promise, following their further development into iterated complexes capable of bridging two  $M_b$  magnetic ions, for use as synthons for building magnetic crystals where one would be able to predetermine the sign of the local exchange interactions and extend these globally to the crystal and also to learn how

to also control the magnitude of the exchange coupling interactions. While it was understood that the idea could meet its demise at the hands of other bridging interactions, such as those of  $\pi$ -symmetry, it was hoped that such work would lead to valuable contributions to the intellectually striking and well-established field of research which was at the time and is to this day targeting synthetically designed magnetic crystals.

The challenges became those of showing that this idea was valid in some multimetallic ion and also of designing  $(M_a)_2PAC$  systems with internally aligned spins that could bridge  $M_b$  ions as an approach to designed magnetic crystals. It was further rationalized that the bonding to  $M_b$  of the  $(M_a)_2PAC$  bridging complexes would need to be weak so that growing crystals would be able to heal imperfections during a not too exothermic growth process as an essential condition for obtaining designed magnetic crystals of reasonable size. This work, of course, required much deliberation on the chemical, structural and electronic requirements of the  $(M_a)_2PAC$  systems and on the magnetic crystals that might result before they were ever created in practice, and it was additionally satisfying because it was being carried out in the context of an international field that is nothing less than an intellectual banquet. Reasonable progress was made in showing the idea concerning the control of the sign of exchange coupling has validity in real systems via the multimetallic ion  $\{Co^{II}[Co^{III}(PAC)]_3\}^-$ . Significant advances were made in moving toward  $(M_a)_2PAC$  species that looked suitable for building designed magnetic crystals. A one-dimensional chain based on  $[Mn^{III}(PAC)]^-$  was adventitiously discovered. This work is highlighted in several places in the review, especially near the end.

However, this most stimulating area of the design of magnetic crystals with its uncompromising demands for full-time intellectual and experimental engagement had to be terminated in the 1990s. This was required by two developments. First, there was the need to focus on oxidation catalysis following the discovery of working Fe-TAML catalysts with their own obdurate demands for focus. Second, the field of green chemistry began emerging in the early 1990s, inspired by Paul Anastas, and the Fe-TAML program fitted with it perfectly in rationale and objective. Thus, in the most rewarding of all developments in our program, green chemistry became a central passion in the early 1990s with Carnegie Mellon University having the first course in the area starting in 1992 and the Professor Collins' group spending much of its time focusing on understanding how to engage effectively in the extraordinarily broad challenges involved with building a field of chemistry aimed at no less than constructing the chemical dimension of a sustainable high-technology civilization.

Catalysis-related features of the iron complexes in different oxidation states have been recently reviewed [16]. This account collects and reviews the chemistry of the other first-row transition metal complexes that has been important in the evolution of the Fe-TAML activators. It opens with a brief description of the Collins ligand systems, followed by a survey of mononuclear metal complexes focusing on their structural features, spectroscopic characterization, and catalytic activity. A sizable section is focused on countering a recent article contesting the innocence

of the TAML system designed by the Collins Group to be innocent. In this section, we also thank the authors of the contesting article for showing TAML systems can be excellent  $\pi$ -donors. A description of polynuclear compounds with an emphasis on their magnetic properties and design considerations concludes the review. Many results were obtained before the density functional theory (DFT) revealed its significant prediction potential. Therefore, some of the systems have been probed by DFT [17] and these results are also included here for the first time.<sup>1</sup>

## 2. A ligand survey

For the purposes of this review, a new nomenclature is introduced (Table 1) to differentiate easily the many different chelating systems. Development of the ligating systems discussed here commenced in 1980 and the first complexes were introduced in the literature in 1984 by the example of the PAC type  $H_4L$  and  $H_4P$  ligands (Table 1) [18]. Their acyclic systems contain two amido ( $N$ ) and two alkoxido or phenolato ( $O$ ) donor centers ( $2N/2O$ ;  $H_4L$  and  $H_4P$ , respectively). When protonated, these neutral  $N-H$  and  $O-H$  functionalities are weak ligands with the protonated amide functional groups engaging where possible in  $O$ -coordination, but they transform into very powerful negatively charged, predominantly  $\sigma$ -donating amido- $N$  ligands upon deprotonation. The overall ligand charge of  $-4$  also makes the ligands particularly suitable for metal centers in higher oxidation states. Though transition metal salts in lower oxidation states have often been used as starting materials during the syntheses, the metal oxidation states in the stable isolated complexes are normally higher. This general feature was in fact predicted. The  $\sigma$ -donor centers additively enforce a significant decrease in the redox potentials of the complexes [19] such that low-valent species, deriving from low-valent metal ions used for insertions, once formed can be oxidized rapidly by a variety of components of the reaction media, including dioxygen, where it has not been excluded, as well as by deliberately added more powerful oxidizing agents such as hydrogen peroxide, *tert*-butyl hydroperoxide, peroxy acids, or diacylperoxides. Because of their special significance in oxidation chemistry, it is worth pointing out that such added oxidizing agents are required to date for the formation of terminal oxo complexes, but the intermediate formation of iron(V)oxo complexes is implied in the chemistry of iron(III)-TAML complexes with dioxygen in weakly coordinating solvents where the products are  $\mu$ -oxo- $[Fe(IV)(Q)]_2$  complexes [9]. The conceptual merger of two  $H_4L$  ligand systems gave rise to the binucleating ligands  $H_8L'$  and  $H_8L''$  (Table 1), the prototype  $(M_a)_2PAC$  complexes introduced above, produced with the design of molecule-based magnetic

<sup>1</sup> Density functional calculations were performed using Becke's three-parameter hybrid functional (B3LYP) and basis set 6-31G, unless stated otherwise, provided by the Gaussian 03 (release B.05) software package. Geometry optimizations were terminated upon reaching the default convergence criteria. Mulliken population analysis was employed to monitor the electron distribution. The SCF calculations used tight convergence criteria ( $10^{-6}$  root mean square, RMS, deviation in the density matrix and  $10^{-8}$  atomic unit maximum deviation in energy).

Table 1  
The ligand systems designed and discussed in this review

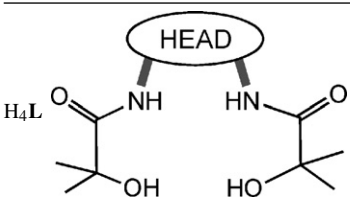
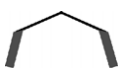

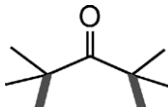

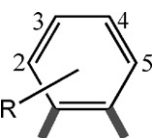
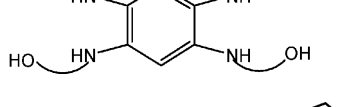

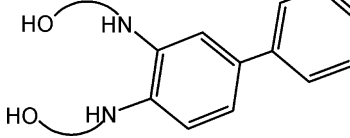

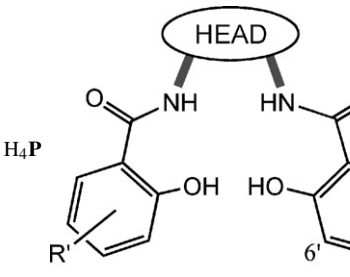


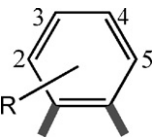
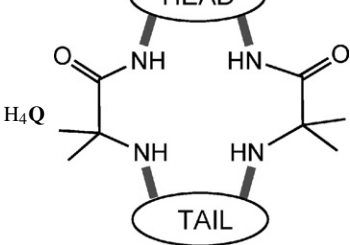
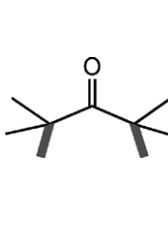

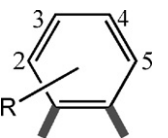
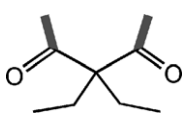

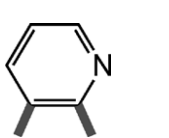
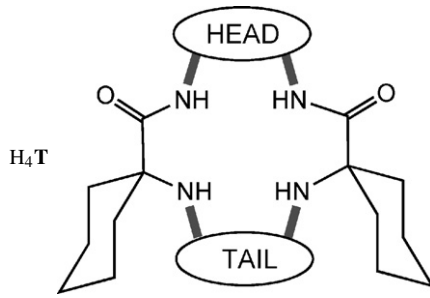
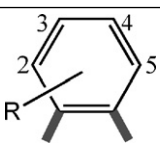
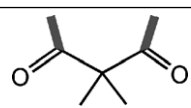
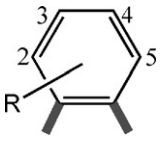

Ligand system	Abbreviation	Head	Tail	R/R'
	H <sub>4</sub> L <sup>1</sup>		n/a	n/a
	H <sub>4</sub> L <sup>2</sup>		n/a	n/a
	H <sub>4</sub> L <sup>3</sup> H <sub>4</sub> L <sup>4</sup>		n/a	H/— 3,4-Cl <sub>2</sub> /—
	H <sub>8</sub> L'		n/a	n/a
	H <sub>8</sub> L''		n/a	n/a
	H <sub>4</sub> P <sup>1</sup>		n/a	—/4',6'-Cl <sub>2</sub>
	H <sub>4</sub> P <sup>2</sup> H <sub>4</sub> P <sup>3</sup> H <sub>4</sub> P <sup>4</sup>		n/a	H/H H/4',6'-Cl <sub>2</sub> 3,4-Cl <sub>2</sub> /4',6'-Cl <sub>2</sub>
	H <sub>4</sub> Q <sup>1</sup>		n/a	n/a
	H <sub>4</sub> Q <sup>2</sup> H <sub>4</sub> Q <sup>3</sup> H <sub>4</sub> Q <sup>4</sup> H <sub>4</sub> Q <sup>5</sup>			H/— 3,4-Cl <sub>2</sub> /— 3,4-(OMe) <sub>2</sub> /— 3,4-Me <sub>2</sub> /—
	H <sub>4</sub> Q <sup>6</sup>		n/a	n/a

Table 1 (Continued)

Ligand system	Abbreviation	Head	Tail	R/R'
	H <sub>4</sub> Q <sup>7</sup> H <sub>4</sub> Q <sup>8</sup> H <sub>4</sub> Q <sup>9</sup>			H/ 3,4-Cl <sub>2</sub> /– 3,4-(OMe) <sub>2</sub> /–
	H <sub>4</sub> T <sup>1</sup>			H/–
	H <sub>4</sub> T <sup>2</sup> H <sub>4</sub> T <sup>3</sup>			3,4-Cl <sub>2</sub> /– 3,4-(OMe) <sub>2</sub> /–

materials in mind. The binding of two paramagnetic metal ions led to ideal systems for the study of exchange interactions through extended ligand bridges and for the exploration of the production of magnetic crystals [20].

The 2*N*/2*O* donor system realized in the open H<sub>4</sub>L ligands ruled out cyclization while retaining high-negative charge, so no 2*N*/2*O* macrocyclic ligands were synthesized. One obstacle is the valency limitation of the oxygen phenolato and alkoxido ligands. However, nitrogen provides the extra valency required for forming macrocycles and therefore a crucial switch to the 4*N* tetraamido system was made in 1991 by which time it had become obvious that the acyclic Collins ligands are limited by a formidable propensity to undergo hydrolysis in their derivative first row complexes, that they can be susceptible to an oxidative chelate ring cleavage when the metal center is oxidizing, and that they can be prone in strongly oxidizing complexes to undergo a non-planar amidato-*N* ligand formation that reverses upon reduction of the metal [5]. With regard to the second limitation, the following of the Design Protocol led to the realization that the oxidative ring cleavage could be obviated by the transition from an alkoxido-*O* to an amidato-*N* donor, as this change reduced from two to one the number of lone pairs on the donor atom while leaving the sole remaining lone pair orthogonal to the  $\sigma$  bond being cleaved by the oxidative process found when two are present, thereby shutting down an essential component of the electron flow that we hypothesized is required for the observed ligand decomposition. When the substitution did indeed result in a much more oxidatively robust chelate system, this understanding was generalized as one of the Collins Rules for protecting chelating ligands from oxidative destruction. The resulting H<sub>4</sub>Q ligands, referred to as the TAML systems, were introduced (Table 1) in answer to these many complications of the acyclic systems that had clearly become impediments to designing functional oxidation catalysts [21,22].

The study of TAMLs containing different “head” and “tail” groups provided a broad spectrum of high-valent metal complexes with unique structural, magnetic, and catalytic properties.

Formally high-valent metal complexes can be rather controversial in terms of the localization of oxidation equivalents, i.e., they could be localized entirely on a central metal, reside on a ligand, or be split between the metal and a ligand. In the context of the subject ligand systems, diverse “head” and “tail” groups (Table 1) are either unable (redox innocent) or able (redox non-innocent) to distribute significant positive charge to the point of holding full oxidation equivalents on the ligands via the  $\pi$  network. This is somewhat of a murky area as delocalization can result in a continuum between the two extremes of localized oxidation, metal or ligand, and there is no general acceptance of the amount of deviation from the localized states that represent the turning points when one should consider the innocent ligand becomes non-innocent and visa versa. But the lack of a chain of conjugation and/or aromatic fragments, as in H<sub>4</sub>Q<sup>1</sup>, preserves ligand redox innocence and all oxidation equivalents are localized on the metal center [22]. As the reader will see in Section 3.4, this property of H<sub>4</sub>Q<sup>1</sup> has been contested, but we will argue that H<sub>4</sub>Q<sup>1</sup> is, in fact, an innocent ligand system.

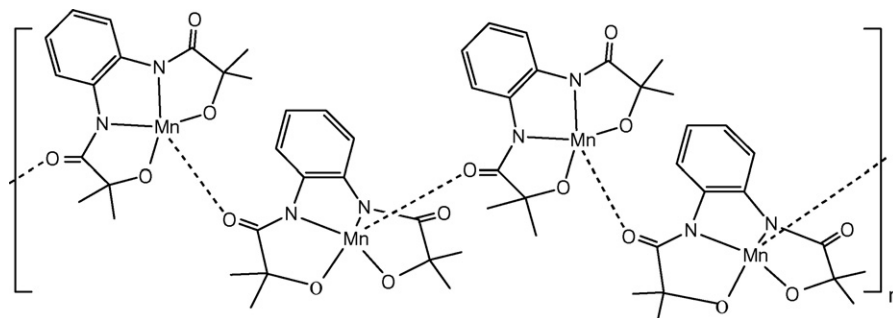
### 3. High-valent mononuclear complexes

Complexes of Mn, Co, Ni, Cr, and Cu in high-oxidation states stabilized by the ligands summarized in Table 1, were characterized by <sup>1</sup>H NMR, IR, Resonance Raman (RR), UV–vis, cyclic voltammetry (CV), and EPR data. Many structures were confirmed by X-ray crystallography. Their main features are described below.

#### 3.1. Manganese complexes

The complex [Mn<sup>V</sup>O(L<sup>3</sup>)]<sup>–</sup> was the first example of a structurally characterized species with a stable Mn<sup>V</sup>=O unit [23]. It was synthesized from the corresponding [Mn<sup>III</sup>(L<sup>3</sup>)]<sup>–</sup> precursor using *tert*-butyl hydroperoxide as the oxidizing agent. Also notable was the polymeric motif of [Mn<sup>III</sup>(L<sup>3</sup>)]<sup>–</sup> in the solid state; the high affinity of Mn<sup>III</sup> towards the oxygen led





Scheme 1. Schematic diagram for the polymeric chain formed by  $[\text{Mn}^{\text{III}}(\text{L}^3)]^-$  in the solid state. The closest intra- and inter-chain Mn–Mn separations equal 5.89 and 8.72 Å, respectively.

to a polymeric network (Scheme 1). This polymeric structure vanished upon the formation of the  $\text{Mn}^{\text{V}}=\text{O}$  unit when one of the two axial sites became occupied by the oxo ( $\text{O}^{2-}$ ) ligand perhaps because of a major attenuation in the axial Lewis acidity produced by the oxo ligand, but crystallization energetics are also in play. The X-ray structure of  $[\text{Mn}^{\text{V}}\text{O}(\text{L}^3)]^-$  showed all four equatorial donor atoms (2N/2O) to be almost planar (RMS deviation from the plane equals 0.003 Å). The square-pyramidal compound was diamagnetic (low spin,  $d^2$ ) with the  $\text{Mn}^{\text{V}}$  center out of the 2N/2O plane by 0.620 Å. A very short manganese–oxygen bond distance (1.548 Å) was consistent with a triple bond  $\text{Mn}^{\text{V}}=\text{O}$  formulation [24]. No benzene ring distortion was observed. This ruled out any cation radical character of the complex and justified the  $\text{Mn}^{\text{V}}$  assignment.

Since  $[\text{Mn}^{\text{V}}\text{O}(\text{L}^3)]^-$  was unstable in water, and especially because the formation of stable mononuclear iron coordination complexes had eluded us with this acyclic tetradentate ligand family, the new class of macrocyclic ligands,  $\text{H}_4\text{Q}$ , containing four amide nitrogen atoms was designed and introduced. Beautiful comprehensive studies of a binucleating Schiff base manganese complex show, inter-alia, another type of aqueous vulnerability [25]. A series of diamagnetic  $[\text{Mn}^{\text{V}}\text{O}(\text{Q})]^-$  complexes was synthesized from  $\text{H}_4\text{Q}$ ,  $\text{Mn}(\text{acac})_3$ , and *tert*-butyl hydroperoxide without isolating the  $\text{Mn}^{\text{III}}$  precursors. The X-ray structural investigation of  $[\text{Mn}^{\text{V}}\text{O}(\text{Q}^3)]^-$  revealed a manganese–oxo bond distance similar to that in  $[\text{Mn}^{\text{V}}\text{O}(\text{L}^3)]^-$  (Table 2). The four amide nitrogen atoms were in one plane (RMS 0.026 Å) with the Mn center located 0.600 Å out of the plane. Oxygen-18 labeled complexes  $[\text{Mn}^{\text{V}}(^{18}\text{O})(\text{L}^3)]^-$  obtained by exchange of the  $^{16}\text{O}$  oxo ligand with  $^{18}\text{O}$  from  $\text{H}_2^{18}\text{O}$  were used to assign by infrared spectroscopy the  $\nu_{\text{Mn}=\text{O}}$  stretching frequencies. Data for structurally related  $[\text{Mn}^{\text{V}}\text{O}(\text{Q})]^-$  complexes showed a  $9\text{ cm}^{-1}$  shift in the stretching frequency along with  $\lambda_{\text{max}}$  shift on moving from  $[\text{Mn}^{\text{V}}\text{O}(\text{Q}^3)]^-$  to  $[\text{Mn}^{\text{V}}\text{O}(\text{Q}^4)]^-$ . The reduction potentials of the  $[\text{Mn}^{\text{V}}\text{O}(\text{Q})]^-$  complexes were also affected by the substituents; a 0.690 V cathodic shift was observed on going from the chloro to the methoxy ring-substituted species.

In the absence of available X-ray structural information, DFT studies allowed the electronic effects brought about by different substituents in the phenyl ring of the  $[\text{Mn}^{\text{V}}\text{O}(\text{Q}^{2-5})]^-$  to be probed. The validity of the DFT model used was evaluated by comparing the geometry of the optimized structure and the available X-ray data for  $[\text{Mn}^{\text{V}}\text{O}(\text{Q}^3)]^-$  (Table 2).

Unlike highly reactive porphyrin and salen based  $\text{Mn}^{\text{V}}$ -oxo systems [26–28], the  $\text{H}_4\text{L}$  and  $\text{H}_4\text{Q}$  based  $\text{Mn}^{\text{V}}$ -oxo complexes,  $[\text{Mn}^{\text{V}}\text{O}(\text{L})]^-$  and  $[\text{Mn}^{\text{V}}\text{O}(\text{Q})]^-$ , showed a limited oxygen transfer capability towards olefins. This was attributed to the high-negative charge and strong  $\sigma$ -donating capacity of the deprotonated amide nitrogen atoms of  $\text{H}_4\text{Q}$ s. This feature presumably makes the oxo ligand significantly less electrophilic and hence less reactive. To enhance the electrophilicity, a new ligand system  $\text{H}_4\text{Q}^6$  containing a pyridine ring instead of the phenyl ring, referred to as “switch” [29], was introduced. It was anticipated that the pyridine N-donor center and its adjacent amidato-O atom would chelate Lewis acids and therefore the electrophilicity of the oxo ligand would be higher. The complex  $[\text{Mn}^{\text{V}}\text{O}(\text{Q}^6)]^-$  was prepared from the  $\text{Mn}^{\text{III}}$  precursor and *tert*-butyl hydroperoxide [29]. Its X-ray structural investigation (Fig. 1) showed geometric similarities with  $[\text{Mn}^{\text{V}}\text{O}(\text{Q}^3)]^-$  (Table 2). Binding of cations to  $[\text{Mn}^{\text{V}}\text{O}(\text{Q}^6)]^-$  in  $\text{CH}_3\text{CN}$  was confirmed by UV–vis,  $^1\text{H}$  NMR,  $^{13}\text{C}$  NMR, and CV studies. The cations  $\text{Li}^+$ ,  $\text{Na}^+$ ,  $\text{Ba}^{2+}$ ,  $\text{Zn}^{2+}$ ,  $\text{Mg}^{2+}$ , and  $\text{Sc}^{3+}$  induced observable spectral changes. IR spectra of  $[\text{Mn}^{\text{V}}(^{18}\text{O})(\text{Q}^6)]^-$  in the presence of  $\text{Li}^+$  or  $\text{Zn}^{2+}$  showed a  $15\text{ cm}^{-1}$  blue shift for the  $\nu_{\text{Mn}=\text{O}}$  bond (from 939 for the  $[\text{Mn}^{\text{V}}(^{18}\text{O})(\text{Q}^6)]^-$  to  $954\text{ cm}^{-1}$ ), demonstrating a decrease in the donor capacity of the macrocyclic ligand due to the cation binding. A three or 1250-fold rate

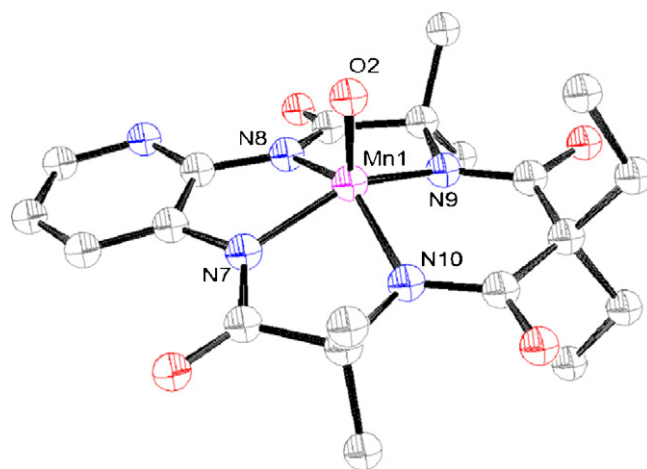


Fig. 1. X-ray crystal structure of  $[\text{Mn}^{\text{V}}\text{O}(\text{Q}^6)]^-$ . Selected bond lengths (Å): Mn–O(2), 1.549(3); Mn–N(7), 1.884(4); Mn–N(8), 1.873(3); Mn–N(9), 1.881(3); Mn–N(10), 1.885(3).

Table 2  
Selected structural, spectral, and DFT computed properties of some manganese(V)-oxo complexes

Complex	Bond distances (Å)		Out of plane shift (Å)	$\nu(\text{Mn}-^{16}\text{O}/\text{Mn}-^{18}\text{O})$ (cm <sup>-1</sup> )		Mulliken charge <sup>a</sup>	
	Mn–O <sub>axial</sub>	(Mn–N <sub>eq</sub> ) <sub>avg</sub>		IR	RR	Mn	O
[Mn <sup>V</sup> O(L <sup>3</sup> )] <sup>-</sup>	1.548(4)	1.872, 1.828 <sup>b</sup>	0.620	–	–	–	–
[Mn <sup>V</sup> O(Q <sup>3</sup> )] <sup>-</sup>	1.555(4)	1.878, 1.900	0.600	979/942	981/942	–	–
	1.563 <sup>a</sup>	1.891, 1.896	–	–	–	1.251	–0.393
[Mn <sup>V</sup> O(Q <sup>2</sup> )] <sup>-</sup>	1.565 <sup>a</sup>	–	–	972/934	972/934	1.245	–0.402
[Mn <sup>V</sup> O(Q <sup>5</sup> )] <sup>-</sup>	1.566 <sup>a</sup>	–	–	973/936	976/939	1.244	–0.402
[Mn <sup>V</sup> O(Q <sup>4</sup> )] <sup>-</sup>	1.567 <sup>a</sup>	–	–	970/933	973/933	1.245	–0.402
[Mn <sup>V</sup> O(Q <sup>6</sup> )] <sup>-</sup>	1.549(3)	1.884, 1.873	0.579	–/939	–	–	–
	1.563 <sup>a</sup>	1.897, 1.893	–	–	–	–	–
[Mn <sup>V</sup> O(Q <sup>6</sup> -Li)]	1.559 <sup>a</sup>	–	–	–/954	–	1.260	–0.369
[Mn <sup>V</sup> O(Q <sup>6</sup> -Na)]	1.560 <sup>a</sup>	–	–	–	–	1.263	–0.371
[Mn <sup>V</sup> O(Q <sup>6</sup> -Zn)] <sup>+</sup>	1.560 <sup>a</sup>	–	–	–/954	–	1.259	–0.354

<sup>a</sup> Calculated by DFT.

<sup>b</sup> Mn–O<sub>eq</sub> distance.

increase for the Ph<sub>3</sub>P oxidation into Ph<sub>3</sub>P=O by [Mn<sup>V</sup>O(Q<sup>6</sup>)]<sup>-</sup> was observed in the presence of five equivalents of Na<sup>+</sup> or Sc<sup>3+</sup>, respectively.

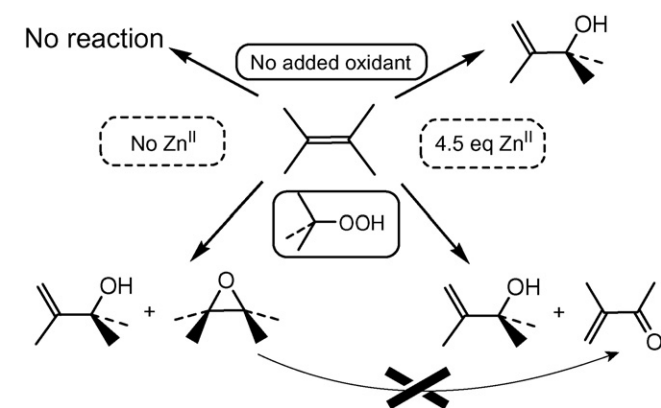
Induced by Zn<sup>2+</sup>, oxidation of 2,3-dimethyl-2-butene by [Mn<sup>V</sup>O(Q<sup>6</sup>)]<sup>-</sup> produced the allylic alcohol derivative, 2,3-dimethylbut-1-en-3-ol. There was no reaction in the absence of Zn<sup>2+</sup> (Scheme 2). In the presence of excess *tert*-butyl hydroperoxide, the formation of 2,3-dimethylbut-1-en-3-ol (~95%) and 2-methyl-1-butene-3-one was observed only with Zn<sup>2+</sup>, whereas 2,2,3,3-tetramethyloxirane and 2,3-dimethylbut-1-en-3-ol were formed in the absence of cations indicating different reaction mechanisms [29]. When [Mn<sup>V</sup>(<sup>18</sup>O)(Q<sup>6</sup>)]<sup>-</sup> (ca. 27% by ESI-MS) was used in the reaction, both the allylic alcohol and the ketone contained <sup>18</sup>O label (ca. 8% by GC–MS), suggesting that the olefin oxidation followed an O-transfer mechanism involving [Mn<sup>V</sup>O(Q<sup>6</sup>)]<sup>-</sup>.

The DFT simulation of the binding of Li<sup>+</sup> to [Mn<sup>V</sup>O(Q<sup>6</sup>)]<sup>-</sup> employing a simplified [Q<sup>6</sup>]<sup>4-</sup> structure with the ethyl groups replaced by hydrogen atoms, suggests the chelation by the pyridine nitrogen and adjacent amide oxygen atom (Fig. 2). The

Li–N<sub>pyr</sub> and Li–O<sub>amide</sub> bond distances were 1.979 and 1.886 Å, respectively. The binding does not perturb the overall structural integrity of the molecule. Elongation of the Mn–N<sub>amide</sub> (1.937 versus 1.884 Å) and C=O<sub>amide</sub> bonds (1.286 versus 1.251 Å) and shortening of the N–C<sub>amide</sub> bond (1.338 versus 1.376 Å) were observed. These changes, also found for Na<sup>+</sup> and Zn<sup>2+</sup>, were rationalized in terms of the electron-withdrawing effect of the bound cation. DFT calculations also suggest that binding of cations increased the positive charge at both manganese and oxygen, thus enhancing the electrophilicity of the oxo ligand. The effect is more pronounced for the divalent cations (Zn<sup>2+</sup>) than monovalent ones (Li<sup>+</sup> and Na<sup>+</sup>). These results agree with the observed increase in the oxygen transfer reactivity of the complexes towards 2,3-dimethyl-2-butene and PPh<sub>3</sub>.

### 3.2. Cobalt complexes

The first Co<sup>IV</sup> complexes of H<sub>4</sub>P ligands were obtained by Ce<sup>IV</sup> oxidation of the corresponding stable Co<sup>III</sup> octahedral



Scheme 2. Oxidation pathways of 2,3-dimethyl-2-butene in the presence of [Mn<sup>V</sup>O(Q<sup>6</sup>)]<sup>-</sup> at 50 °C. Without oxidant the ratio of [Mn<sup>V</sup>O(Q<sup>6</sup>)]<sup>-</sup>/olefin was 1:11; under catalytic conditions the ratio of [Mn<sup>V</sup>O(Q<sup>6</sup>)]<sup>-</sup>/olefin/<sup>t</sup>BuOOH was 1:132:266.

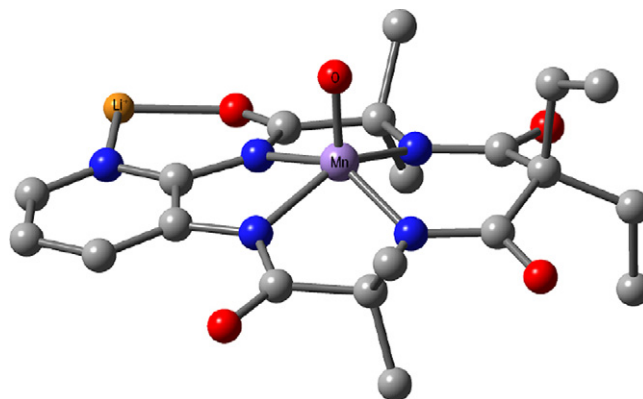
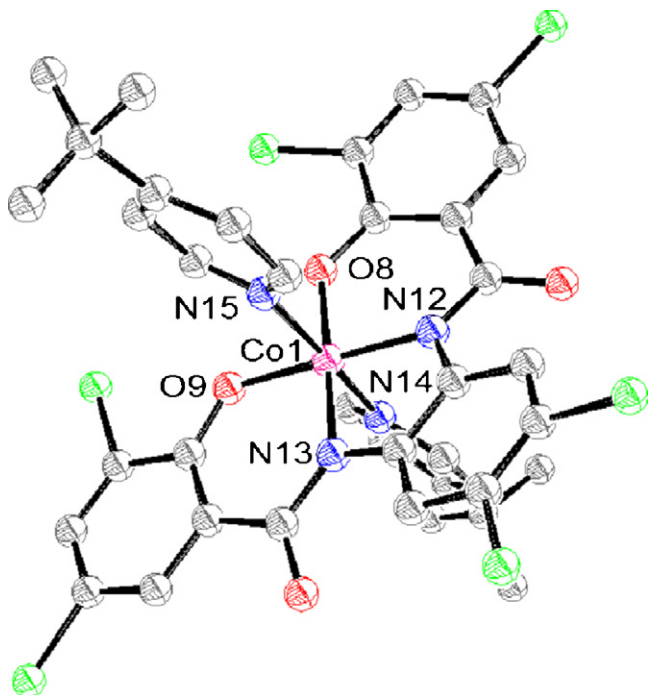
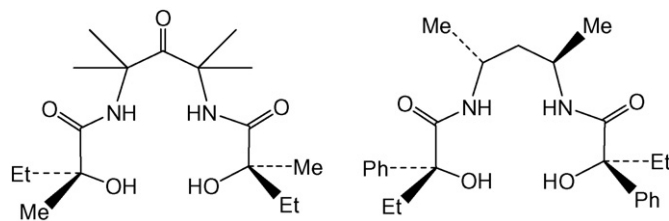


Fig. 2. Structure of [Mn<sup>V</sup>O(Q<sup>6</sup>-Li)] suggested by DFT (purple: manganese; blue: nitrogen; red: oxygen; yellow: lithium). Selected bond distances are given in Table 2. Hydrogen atoms are not shown for clarity. (For interpretation of the references to color in this figure legend, the reader is referred to the web version of the article.)

Fig. 3. X-ray crystal structure of  $[\text{Co}(\text{P}^4)(t\text{-Bu-4-py})_2]$ .

complexes [30]. The X-ray crystal structure of the octahedral complex  $[\text{Co}^{\text{IV}}(\text{P}^4)(4\text{-}^t\text{Bupy})_2]$  is shown in Fig. 3. The EPR data and magnetic susceptibility measurements indicated a low spin  $S=1/2$   $\text{Co}^{\text{IV}}$  species as the most likely formulation, although ligand non-innocence was also considered to be a possible role player giving a significantly ligand-located oxidation site. Indeed, there are strong suggestions in this review based upon the electronic structures determined for other Co complexes of non-innocent ligands that a  $\text{Co}^{\text{III}}$ -ligand radical species is a more likely formulation. The cyclic voltammogram of  $[\text{Co}^{\text{IV}}(\text{P}^4)(4\text{-}^t\text{Bupy})_2]$  showed two reversible features at +0.390 and +0.840 V versus  $\text{Fc}^+/\text{Fc}$  attributed to  $\text{Co}^{\text{IV/III}}$  and another process. The  $[\text{Co}^{\text{IV}}(\text{P}^4)(4\text{-}^t\text{Bupy})_2]$  complex generated electrochemically was identical to that obtained by  $\text{Ce}^{\text{IV}}$  oxidation.

The tetra-anionic alkoxido ligands derived from  $\text{H}_4\text{L}$  ligands are stronger electron donors than those derived from the phenolato  $\text{H}_4\text{P}$  ligands. The large variation in the donor capacities is an underlying factor responsible for the differences in the chemical behavior of these  $\text{Co}^{\text{III}}$  centers. The phenolato and alkoxido ligands coordinate  $\text{Co}^{\text{III}}$  to generate stable octahedral (pyridine derivatives as axial ligands) and square planar metal center geometries (with weak axial Lewis acidities), respectively. A

Fig. 4. Structures of modified  $\text{H}_4\text{L}^2$  and  $\text{H}_4\text{L}^1$  ligands.

simple intuitive way to think about this is to consider that the metal, as a Lewis acid, is looking to have its acidity quenched by ligands. Starting from a six-coordinate complex and increasing the equatorial Lewis basicity, the system will reach a point where the Lewis acidity of the metal is quenched such that the axial ligands can be released and the stable complexes become five- or four-coordinate. Considering that the vast majority of  $\text{Co}^{\text{III}}$  complexes are octahedral, the stable square planar  $\text{Co}^{\text{III}}$  configuration of  $[\text{Co}^{\text{III}}(\text{L}^{2,3})]^-$  provides a further indication of the unusually high-donor capacities of these Collins ligands [28,31,32]. The X-ray crystal structures showed shorter Co–O and Co–N bond distances when compared to either octahedral  $\text{Co}^{\text{III}}$  or square planar  $\text{Co}^{\text{II}}$  complexes of related ligands [33]. Solid-state magnetic data and  $^1\text{H}$  NMR measurements (in  $\text{CD}_2\text{Cl}_2$ ) supported the assignment of a spin triplet ( $S=1$ ) ground state for both complexes. When a  $\text{CD}_3\text{OD}$  solution of square planar  $\text{Na}[\text{Co}^{\text{III}}(\text{L}^2)]$  was treated with two equivalents of KCN, the low-symmetry diamagnetic, octahedral complex  $[\text{Co}^{\text{III}}(\text{L}^2)(\text{CN})_2]^{3-}$  was formed and characterized by  $^1\text{H}$  NMR, IR, and X-ray crystallography [31].

The first neutral square-planar  $\text{Co}^{\text{III}}$  complexes were obtained by alkylation of  $[\text{Co}^{\text{III}}(\text{L}^2)]^-$  and related anionic complexes (Scheme 3). The alkylations occurred cleanly with a variety of alkylating agents [32]. The structure of one alkylated complex was established by  $^1\text{H}$  NMR, IR, and MS data.

The catalytic activity of  $[\text{Co}^{\text{III}}(\text{L}^{1-4})]^-$  and  $[\text{Co}^{\text{III}}(\text{P}^4)]^-$  complexes was tested in the oxidation of styrene to styrene oxide with iodosylarenes in acetonitrile (Table 3) [34]. The  $[\text{Co}^{\text{III}}(\text{L}^2)]^-$  complex showed the highest activity with  $\text{PhIO}$ , to yield 5.5 turnover numbers, 67% conversion of styrene, and 80% of the catalyst remaining at the end of the reaction. Eight different  $\text{Co}^{\text{III}}$  complexes of chiral ligands (Fig. 4) have been used as catalysts for asymmetric epoxidation of ring-substituted styrenes [35]. Reactions were performed in acetonitrile at ca.  $0^\circ\text{C}$  to afford the corresponding oxiranes in 25–86% yield. Regrettably, the highest enantiomeric excess achieved did not exceed 17%.

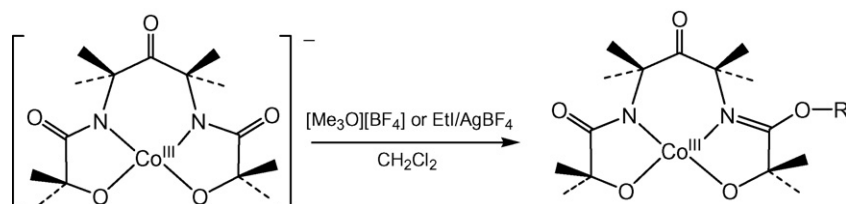
Scheme 3. Alkylation of  $[\text{Co}^{\text{III}}(\text{L}^2)]^-$ .



Table 3

Catalytic oxidation of styrene in the presence of cobalt complexes in acetonitrile

Complex	Oxidant	<i>T</i> (°C)	Conversion (%)	TON	Time (h)
Na[Co <sup>III</sup> (L <sup>2</sup> )]	PhIO	0	56	3.7	1
	PhIO	25	41	2.8	2
	C <sub>6</sub> F <sub>3</sub> IO	0	26	2.0	1
	2,4,6-Me <sub>3</sub> C <sub>6</sub> H <sub>2</sub> IO	0	46	3.2	24
[Ph <sub>4</sub> P][Co <sup>III</sup> (L <sup>2</sup> )]	PhIO	25	37	2.7	22
Na[Co <sup>III</sup> (L <sup>3</sup> )]	PhIO	0	43	2.8	23
Na[Co <sup>III</sup> (L <sup>4</sup> )]	PhIO	0	67	5.5	22
Na[Co <sup>III</sup> (P <sup>1</sup> )]	PhIO	0	25	1.7	45
Na[Co <sup>III</sup> (P <sup>2</sup> )]	PhIO	0	14	1.0	23

The deprotonated H<sub>4</sub>Q<sup>1</sup> ligand provided both an innocent electronic environment and superior oxidative stability and, therefore, was used to stabilize the first reported macrocyclic square planar Co<sup>III</sup> complex [Co<sup>III</sup>(Q<sup>1</sup>)]<sup>−</sup> [22,36]. Similar structures were obtained for the Ni<sup>III</sup> [37] and Cr<sup>V</sup> [38] complexes of this ligand. The <sup>1</sup>H NMR spectra for [Co<sup>III</sup>(Q<sup>1-4</sup>)]<sup>−</sup> showed paramagnetically shifted signals as expected for square planar *S* = 1 systems. The cobalt complexes [Co<sup>III</sup>(Q<sup>2-4</sup>)]<sup>−</sup> were dark purple, stable in aprotic solvents, and hydrolytically stable [39]. These Co<sup>III</sup> complexes were chemically or electrochemically oxidized into stable neutral species, e.g., [Co<sup>III</sup>(Q<sup>3•</sup>)]. The [Co<sup>III</sup>(Q<sup>3•</sup>)] complex was the first crystallographically characterized neutral square planar cobalt species in an oxidation state higher than +2. The structural changes in the macrocycle upon oxidation of [Co<sup>III</sup>(Q<sup>3</sup>)]<sup>−</sup> into [Co<sup>III</sup>(Q<sup>3•</sup>)] indicate a redox non-innocence of the ligand (Table 4). The Mulliken spin populations as obtained from DFT analysis support the *S* = 1 spin state for the cobalt center.

Replacing the *gem*-dimethyl groups with a cyclohexyl ring provided appreciable solubility of [Co<sup>III</sup>(T<sup>1-3•</sup>)] in hydrocarbons (~7.4 versus <0.2 mM for the *gem*-dimethylated analogue [Co<sup>III</sup>(Q<sup>3</sup>)]<sup>−</sup> in cyclohexane) [40]. The blue cobalt complexes [Co<sup>III</sup>(T<sup>1-3•</sup>)] oxidized various substrates in cyclohexane, becoming in the processes Co<sup>III</sup> species which precipitated as fine purple solids. The precipitates were re-oxidized with Br<sub>2</sub> into the original blue neutral species. The [Co<sup>III</sup>(T<sup>1-3</sup>)]<sup>−</sup> complexes showed a reversible oxidation process by cyclic voltammetry, with the formal reduction potentials being 0.580, 0.740, and 0.180 V versus Fc<sup>+</sup>/Fc for the complexes of H<sub>4</sub>T<sup>1</sup>, H<sub>4</sub>T<sup>2</sup>, and H<sub>4</sub>T<sup>3</sup>, respectively. The neutral species [Co<sup>III</sup>(T<sup>2•</sup>)] showed EPR signals (CH<sub>2</sub>Cl<sub>2</sub>, 4 K) at *g* = 2.58, 2.21, and 2.04 due to coupling between the *S* = 1 Co<sup>III</sup> center and the organic radical of the oxidized ligand [31]. The oxidation of tetramethyl-*p*-phenylenediamine, **I**, by [Co<sup>III</sup>(T<sup>2•</sup>)] yielded a charge-transfer, Wurster's Blue radical cation salt

[I<sup>•+</sup>][Co<sup>III</sup>(T<sup>2</sup>)], the EPR spectrum of which (CH<sub>2</sub>Cl<sub>2</sub>, 4 K) showed only the diagnostic *g* = 2.00 signal of the organic radical [31]. Oxidation of decamethylferrocene and MgTPP by [Co<sup>III</sup>(T<sup>1-3•</sup>)] complexes were also studied [40]. Oxidative coupling reactions converting thiophenol and tributyltin hydride to diphenyl disulfide and the bis(tributyltin) dimer in cyclohexane proceeded quantitatively with <sup>1</sup>H NMR confirmation. Only [Co<sup>III</sup>(T<sup>2•</sup>)] was a sufficiently strong oxidant to convert hydroquinone to quinone [40].

[Co<sup>II</sup>(Q<sup>6</sup>)]<sup>2−</sup> and the crystallographically characterized [Co<sup>III</sup>(Q<sup>6</sup>)]<sup>−</sup> complexes were synthesized according to Scheme 4 [39]. As in the case of [Mn<sup>V</sup>O(Q<sup>6</sup>)]<sup>−</sup>, these complexes bound alkali and alkaline earth cations. Binding of cationic Ru<sup>II</sup> complexes in acetonitrile occurred as well. The electrophilicity of Co<sup>III</sup> in acetonitrile is increased when [(bpy)<sub>2</sub>RuCl<sub>2</sub>].2H<sub>2</sub>O and [(Me<sub>2</sub>bpy)<sub>2</sub>RuCl<sub>2</sub>].2H<sub>2</sub>O interact with the binding site of this switching system. The binding of such Ru<sup>II</sup> species caused a 0.400 V anodic shift for the Co<sup>III/II</sup> couple.

### 3.3. Chromium, nickel, and copper complexes

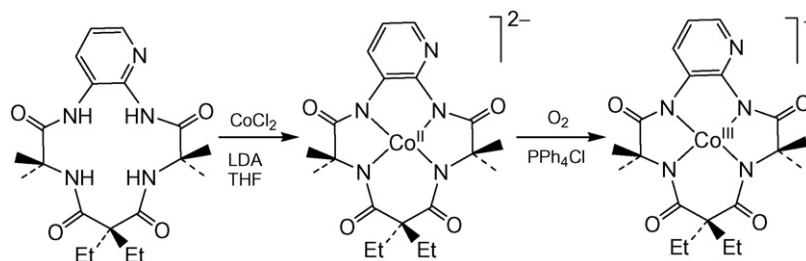
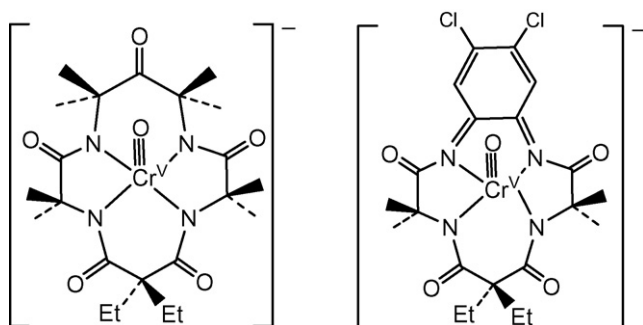
#### 3.3.1. Chromium complexes

Square-pyramidal Cr<sup>V</sup> complexes [Cr<sup>V</sup>O(Q)]<sup>−</sup> of H<sub>4</sub>Q<sup>1</sup> and H<sub>4</sub>Q<sup>3</sup> were obtained using CrCl<sub>2</sub> and *tert*-butyl hydroperoxide (Fig. 5) [38]. H<sub>4</sub>Q<sup>1</sup> is a redox innocent ligand and therefore a formal oxidation state of +5 could be assigned for chromium in [Cr<sup>V</sup>O(Q<sup>1</sup>)]<sup>−</sup>. This assignment is supported by X-ray and EPR data [38]. The Cr–O bond lengths in [Cr<sup>V</sup>O(Q<sup>3</sup>)]<sup>−</sup> and [Cr<sup>V</sup>O(Q<sup>1</sup>)]<sup>−</sup> of 1.569(2) and 1.580(6) Å, respectively, were typical for a Cr<sup>V</sup>≡O formulation [24]. Chromium was located 0.60 Å above the plane containing the four amide nitrogen atoms in [Cr<sup>V</sup>O(Q<sup>3</sup>)]<sup>−</sup>. All four Cr–N bond lengths were similar (avg. 1.913 Å). In contrast, the four nitrogen atoms of [Cr<sup>V</sup>O(Q<sup>1</sup>)]<sup>−</sup> alternated above and below the mean 4*N* plane, probably as a result of the larger macrocycle resulting in a larger coordination

Table 4

Selected X-ray/DFT bond distances (Å) and spin densities for [Co<sup>III</sup>(Q<sup>3</sup>)]<sup>−</sup> and [Co<sup>III</sup>(Q<sup>3•</sup>)]

Complex	Co–N <sub>head</sub>	Co–N <sub>tail</sub>	N <sub>head</sub> –C <sub>phenyl</sub>	C3–C4	Averaged Mulliken spin densities			
					Co	N <sub>head</sub>	C2, C5	C3, C4
[Co <sup>III</sup> (Q <sup>3</sup> )] <sup>−</sup>	1.825(4)/1.840	1.824(4)/1.842	1.410(6)/1.409	1.380(4)/1.393	1.739	0.003	−0.002	0.004
[Co <sup>III</sup> (Q <sup>3•</sup> )]	1.823(4)/1.851	1.805(4)/1.815	1.353(6)/1.371	1.428(10)/1.426	1.629	−0.167	−0.125	−0.103

Scheme 4. Syntheses of  $[\text{Co}^{\text{II}}(\text{Q}^6)]^{2-}$  and  $[\text{Co}^{\text{III}}(\text{Q}^6)]^-$ .Fig. 5. Structures of chromium(V) complexes  $[\text{Cr}^{\text{VO}}(\text{Q}^1)]^-$  and  $[\text{Cr}^{\text{VO}}(\text{Q}^3)]^-$ .

dinating cavity, with chromium being by  $0.58 \text{ \AA}$  out of the plane.

The oxo nature of  $[\text{Cr}^{\text{VO}}(\text{Q})]^-$  complexes was confirmed by the IR data using  $^{18}\text{O}$ -labeled species. The  $\nu_{\text{Cr}=\text{O}}$  band of  $[\text{Cr}^{\text{VO}}(\text{Q}^3)]^-$  was found at  $982$  and  $944 \text{ cm}^{-1}$  for  $^{16}\text{O}$  and  $^{18}\text{O}$  species, respectively. In  $[\text{Cr}^{\text{VO}}(\text{Q}^1)]^-$ , the bands were at  $982$  and  $941 \text{ cm}^{-1}$ , respectively. The EPR spectra of  $[\text{Cr}^{\text{VO}}(\text{Q})]^-$  supported the  $\text{Cr}^{\text{V}}$  formulation. The redox non-innocent  $\text{H}_4\text{Q}^3$  ligand could hold oxidation equivalent/s. The spectra of  $[\text{Cr}^{\text{VO}}(\text{Q}^1)]^-$  and  $[\text{Cr}^{\text{VO}}(\text{Q}^3)]^-$  in  $\text{CH}_3\text{CN}$  at  $294 \text{ K}$  were virtually identical and consisted of a strong nine-line first-derivative signal centered at  $g = 2.006$  due to hyperfine interactions with the four equivalent N donors ( $A^{\text{N}} = 2.7 \text{ G}$ ). A hyperfine interaction with  $^{53}\text{Cr}$  ( $I = 3/2$ ,  $9.54\%$  natural abundance) of  $A^{\text{Cr}} = 17.9 \text{ G}$  produces a weaker four-line feature with each component showing the nitrogen hyperfine interaction as expected for chromium(V) complexes. These oxo complexes provided model systems for the study.

### 3.3.2. Nickel complexes

A square-planar  $\text{Ni}^{\text{III}}$  complex of the redox innocent ligand  $\text{H}_4\text{Q}^1$  was obtained using  $(\text{Ph}_3\text{P})_2\text{NiBr}_2$  and *tert*-butyl hydroperoxide [37]. The amide nitrogen atoms alternated

$0.25 \text{ \AA}$  above and below their mean plane and  $\text{Ni}^{\text{III}}$  sat  $0.09 \text{ \AA}$  out of this plane. The average Ni–N bond distance was  $1.84 \text{ \AA}$ . Addition of cyanide at room temperature in dichloromethane caused a change in color from purple to yellow, offering evidence for the formation of an adduct (1:1) with  $K_{20^\circ\text{C}} = (3.2 \pm 0.9) \times 10^3 \text{ M}^{-1}$ . Similar color changes occurred in the presence of ethanol, pyridine, 2,6-lutidine, and  $\text{Me}_3\text{P}$  at  $77 \text{ K}$ , and suggested that they were caused by changes in the coordination number of nickel. The EPR studies supported this (Table 5). The spectrum of  $[\text{Ni}^{\text{III}}(\text{Q}^1)]^-$  in excess of  $\text{CN}^-$  at  $4 \text{ K}$  was rhombic (in  $\text{CH}_2\text{Cl}_2$  or  $\text{EtOH}$  glass). When  $^{13}\text{CN}^-$  was used, the hyperfine pattern showed only one  $\text{CN}^-$  bound at  $4 \text{ K}$ . The spectrum of  $[\text{Ni}^{\text{III}}(\text{Q}^1)]^-$  at  $5 \text{ K}$  in 2,5- $\text{Me}_2\text{THF}$ /pyridine (2:1) was also rhombic, confirming coordination of one pyridine. The EPR spectra of these glasses have  $g_1 \approx g_2 = g_{\perp} > g_{\parallel} = g_3$  [37].

### 3.3.3. Copper complexes

The strongly donating PAC ligands  $\text{H}_4\text{L}$  and  $\text{H}_4\text{P}$  stabilized  $\text{Cu}^{\text{III}}$  complexes when  $\text{Cu}(\text{OAc})_2$  was used as a starting material [41]. The X-ray crystal structure of  $[\text{Cu}^{\text{III}}(\text{L}^3)]^-$  revealed its square-planar geometry. The Cu–N<sub>amido</sub> bond lengths of  $1.813(4)$  and  $1.804(4) \text{ \AA}$  were similar to those in the  $\text{Cu}^{\text{III}}$  tripeptide complex of tri- $\alpha$ -aminoisobutyric acid [42]. The oxidation state of copper in complexes of potentially redox non-innocent ligands was confirmed by cyclic voltammetry. The  $\text{H}_4\text{L}^3$ ,  $\text{H}_4\text{L}^4$ ,  $\text{H}_4\text{P}^1$ , and  $\text{H}_4\text{P}^4$  ligands have aromatic rings and therefore could be non-innocent.  $\text{H}_4\text{L}^2$  is a ligand without easy-to-oxidize centers; it is structurally similar to  $\text{H}_4\text{Q}^1$  and therefore has been used as a benchmark for all copper complexes. The  $\text{Cu}^{\text{III/II}}$  reduction potential for  $[\text{Cu}^{\text{III}}(\text{L}^2)]^-$  was very low,  $-1.08 \text{ V}$  versus  $\text{Fc}^+/\text{Fc}$  in  $\text{CH}_3\text{CN}$ . This was evidence for the powerful donor capacity of the ligand. The low value ruled out any ligand-centered character, i.e., ligand-oxidized  $\text{Cu}^{\text{II}}$  species. The  $\text{Cu}^{\text{III/II}}$  reduction potentials of other complexes were also low:  $E^\circ/\text{V}$  versus  $\text{Fc}^+/\text{Fc}$   $[\text{Cu}(\text{P}^4)]^-$ ,  $0.025$ ;  $[\text{Cu}(\text{P}^1)]^-$ ,  $-0.140$ ;  $[\text{Cu}(\text{L}^4)]^-$ ,  $-0.920$ ; and  $[\text{Cu}(\text{L}^2)]^-$ ,  $-0.945$ . The possibility of ligand oxi-

Table 5  
EPR parameters of  $\text{Ni}^{\text{III}}$  complexes

Complex	Solvent	$g_1$	$g_2$	$g_3$	$A_1$ (in G)	$A_2$ (in G)	$A_3$ (in G)
$[\text{Ni}^{\text{III}}(\text{Q}^1)(\text{CN})]^{2-}$	$\text{CH}_2\text{Cl}_2$ with excess of $\text{CN}^-$	2.234	2.159	2.019			
$[\text{Ni}^{\text{III}}(\text{Q}^1)(\text{CN})]^{2-}$	$\text{EtOH}$ with excess of $\text{CN}^-$	2.223	2.144	2.010			
$[\text{Ni}^{\text{III}}(\text{Q}^1)(^{13}\text{CN})]^{2-}$	$\text{EtOH}$ with excess of $^{13}\text{CN}^-$	2.223	2.144	2.010	89	83	100
$[\text{Ni}^{\text{III}}(\text{Q}^1)(\text{py})]^-$	2,5- $\text{Me}_2\text{THF}$ /pyridine (2:1)	2.380	2.269	1.994	–	–	25
$[\text{Ni}^{\text{III}}(\text{Q}^1)]^-$	Toluene/ $\text{CH}_2\text{Cl}_2$	2.366	2.303	1.994			

dation cannot be totally ruled out for the  $H_4P$  complexes, but it remains unlikely because of the very low potentials. The formal reduction potentials of copper(III) complexes of  $H_4Q^3$  and  $H_4Q^2$  ligands were  $-0.800$  and  $-0.940$  V, respectively (versus  $Fc^+/Fc$ ) [43] indicating a noticeable influence of the aromatic ring substituents of the macrocycle.

### 3.4. On TAML innocence in $M[MAC^*]$ complexes

In a recent publication entitled “A DFT overview of high-valent iron, cobalt and nickel tetraamidomacrocyclic ligand (TAML) complexes: the end of innocence?”, Conradie, Conradie and Ghosh have challenged the concept of the innocence of  $H_4Q^1$  [44]. A reviewer of our manuscript for this review asked us to critically evaluate this paper and such an evaluation therefore follows. The Ghosh group’s thinking is based on spin density (SD) plots obtained from DFT calculations for  $MQ^1$  complexes of high-valent Fe, Co and Ni, which show through Mulliken population analyses that the metal’s unpaired SD can leak onto the four amide nitrogen atoms through interaction of  $N(p)$  with  $M(d_{xz})$  and  $M(d_{yz})$  orbitals and also to a lesser extent onto the other amide atoms as well as onto axial ligands. The systems considered include examples with small as well as large spin densities on the amido nitrogen atoms (up to 57%). This study certainly provides the clearest evidence to date that the amido ligands of  $MQ^1$  complexes have  $\pi$ -donor properties and, as such, is a genuine contribution to understanding of the electronic structures of  $MQ^1$  complexes. But since the innocence question has been raised as a result of the study, we are left to ask if the results do indeed challenge the innocence of  $[Q^1]^{4-}$  and, inseparably, whether the metal’s formal oxidation state assignment claimed in each of our papers should be reduced. We are left to ask further, what do the interesting theoretical results mean for the broader understanding of the electronic structures of  $MQ^1$  systems and for the interpretation of spectroscopic properties? And perhaps most importantly of all, what might they mean for the reaction chemistry of  $MQ$  complexes?

### 3.5. What do the DFT results mean for the oxidation state assignment at the metal and the related concept of the innocence of $[Q^1]^{4-}$ ?

We fundamentally disagree with the Ghosh group’s conclusion that  $[Q^1]^{4-}$  is a *non-innocent* ligand for reasons that we present hereafter. The atoms of a ligand that are in direct contact with the metal, such as the amido nitrogen atoms of deprotonated  $H_4MAC^*$  ( $[Q^1]^{4-}$ ), are inevitably engaged in bonding interactions with the metal due to significant orbital overlapping. The bonding leads to the calculated spin transfer and, in the cases considered by Conradie et al. [44], is of  $\pi$ -donation character from the amido ligands to the metals. Almost invariably, much larger measures of electron transfer from the Lewis basic coordinating atoms to the Lewis acidic metal ions are enacted within the  $\sigma$ -bonding network. In accepting the current oxidation state formalism, inorganic chemists have chosen to finesse the widely varying  $\sigma$ -donor capacities of ligands of like charge by ignoring them. Why should we treat the  $\pi$ -donor/acceptor differences any

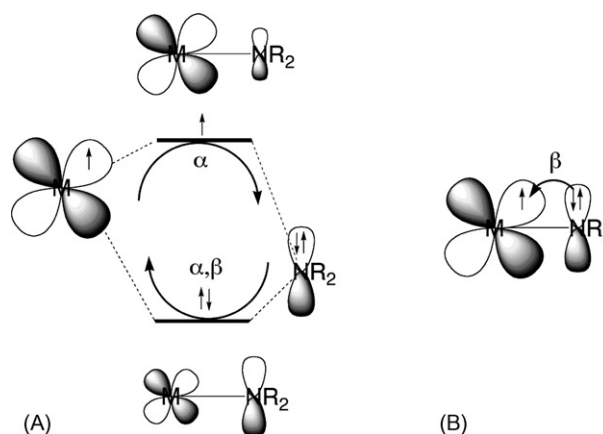


Fig. 6. Diagram (A) illustrates the energetics and transfer of electron density for a three-electron bond between  $M(d\pi)$  and  $N(p\pi)$  orbitals, using a spin-restricted description; the orbital size reflects here the weight in the linear combination. The bonding orbital (doubly occupied) transfers equal amounts of density for the  $\alpha$  and  $\beta$  electrons from the ligand to the metal (lower curved arrow); concomitantly, the antibonding orbital transfers  $\alpha$  density back onto the ligand (upper curved arrow). The net transfer of  $\alpha$  spin density is balanced, because the two  $\alpha$  spin-orbitals are occupied. As a result, there is a net ligand-to-metal transfer of  $\beta$  spin density (diagram B), leading to ligands carrying  $\alpha$  spin density that is of the same sign as present on the metal ion.

differently when these are not coming from a site that is remote from the coordinated atoms where non-innocence is most reasonably invoked, especially when we are dealing with small coordinating atoms and good overlap terms with the metal? We illustrate the spin polarization mechanism in a simplified way, employing only one amido ligand (Fig. 6A) in which the molecular orbital approach shows that the  $N(p\pi)$  orbital is mixing with a metal  $d\pi$  orbital to produce an occupied bonding and a half-occupied antibonding combination (Fig. 6A). Obviously with four amido ligands, the appropriate linear combinations in  $MQ^1$  complexes involve mixing of all the amido  $p\pi$  and the metal  $d\pi$  orbitals. In Fig. 6A, we see that the amido ligand is behaving as a classical  $\pi$ -donor to the metal, giving some electron density to the metal in the bonding orbital and, because the  $d\pi$  orbital is half-occupied, taking only some back in the antibonding orbital. On balance, the interaction gives rise to a net ligand-to-metal transfer of  $\beta$  spin density (Fig. 6B), resulting in a non-vanishing  $\alpha$  spin density at the ligand that is of the same sign as present on the metal. This spin-polarization mechanism is found in virtually all complexes with paramagnetic transition metal ions and suitable donor atoms.

Some of the spin polarizations reported for the  $MAC^*$  complexes by Conradie et al. [44] have been listed in Table 6, together with our results for the anionic complexes  $[Co^{III}F_6]^{3-}$  and  $[Co^{IV}F_6]^{2-}$ . The former anion is found in the solid  $K_3CoF_6$  and has a high-spin ( $S=2$ ) ground state, both computationally and experimentally [45,46]; the latter anion has computationally a low spin ( $S=1/2$ ) ground state, albeit by a small margin, but has been analyzed in the high-spin ( $S=5/2$ ) state for the sake of comparison in Table 6. The comparison shows a dramatic increase in the spin polarization of the ligands upon increasing the oxidation state of cobalt from III to IV. The increase correlates with a shortening of the Co–F bond by 0.1 Å. This is the

Table 6  
Charge and spin densities at metal coordinating atoms from Mulliken population analysis

Compound	d <sup>i</sup>	Spin	Total SD	Charge	Lig. SD	SD (%)	Fe-L (Å)	Reference
[Fe <sup>IV</sup> (MAC*)( <sup>t</sup> BuNC) <sub>2</sub> ]	d <sup>4</sup>	1	2	−0.50 <sup>a</sup>	0.144 <sup>a</sup>	<b>29</b> <sup>b</sup>	1.94 <sup>a</sup>	[44]
Co <sup>IV</sup> (MAC*)(py) <sub>2</sub>	d <sup>5</sup>	1/2	1	−0.53 <sup>a</sup>	0.142 <sup>a</sup>	<b>57</b> <sup>b</sup>	1.88 <sup>a</sup>	[44]
[Co <sup>III</sup> F <sub>6</sub> ] <sup>3−</sup>	d <sup>6</sup>	2	4	−0.80 <sup>c</sup>	0.115 <sup>c</sup>	<b>17</b> <sup>d</sup>	1.99 <sup>c</sup>	This work <sup>e</sup>
[Co <sup>IV</sup> F <sub>6</sub> ] <sup>2−</sup>	d <sup>5</sup>	5/2 <sup>f</sup>	5	−0.64 <sup>g</sup>	0.256 <sup>g</sup>	<b>31</b> <sup>d</sup>	1.89 <sup>g</sup>	This work <sup>e</sup>

<sup>a</sup> Averages for charge, SD, and Fe–N distance taken over four amido nitrogen atoms of MAC\*.

<sup>b</sup> Sum of SDs at four amido nitrogen atoms of MAC\* as a percentage of total SD.

<sup>c</sup> Averages for charge, SD, and Co–F distances taken over six F ligands of a slightly Jahn-Teller distorted octahedron.

<sup>d</sup> Sum of SDs at the six F ligands as a percentage of the total SD.

<sup>e</sup> Results at optimized structure obtained with B3LYP/6-311G for spin state indicated.

<sup>f</sup> The calculations predict an *S* = 1/2 ground state for this complex.

<sup>g</sup> Charge, SD, and Co–F distance at one of the six identical fluorides.

trend expected to be exhibited by the spin polarization mechanism described in Fig. 6. Although we can all almost certainly agree that fluoride is the quintessential innocent ligand, the spin polarizations of this ligand in [Co<sup>IV</sup>F<sub>6</sub>]<sup>2−</sup> are similar to those for the purportedly non-innocent amido nitrogen atoms in the MAC\* species (see below).<sup>2</sup> This example clearly shows that spin densities at the metal-coordinating atoms of a ligand are an improper measure for establishing redox non-innocence of that ligand. Moreover, this type of  $\pi$ -donation has long been part of fundamental electronic structure thinking in coordination chemistry. For example, it is invoked to help explain the ordering of the spectrochemical series and in exactly this way can be invoked to explain the high-spin configuration for K<sub>3</sub>Co<sup>III</sup>F<sub>6</sub>.<sup>3</sup> And if the  $\pi$ -SD found on the amido ligands of MQ<sup>I</sup> complexes should be taken to specify an affirmative answer to Professor Ghosh's title question, "The end of innocence?", then it may as well also be taken to stipulate the end of the oxidation state formalism.

To validate the spin polarization model of Fig. 6, we have performed a detailed Mulliken population analysis based on the DFT calculation for [Co<sup>IV</sup>F<sub>6</sub>]<sup>2−</sup> (Fig. 7). Out of a total electron density of 2.1 transferred from the fluorides to the metal, 1.6 is from  $\beta$  electron density accepted by 3d $\beta$  orbitals. This transfer accounts for the positive ligand spin density of about 1.6 ( $\approx 6 \times 0.26$ ; cf. Fig. 7) and confirms the spin-polarization model of Fig. 6. The  $\sigma$  and  $\pi$  donations contribute about equally to the spin polarization of the ligands. These donations are not normally considered to represent a redox process in the same way that, say, a porphyrin ligand can reduce an oxidized metal ion from a delocalized and overall remote region to produce what is best considered to be a porphyrin ligand radical cation and a one-electron reduced metal. Due to their remoteness, the redox orbitals in such cases are weakly coupled to the metal

and retain their original character in the interaction (see Fig. 8). The transfer, normally of a full electron, is now driven by the energy difference between the ligand and metal orbitals (Fig. 8) and not by overlap interactions between these orbitals as in the case of the MAC\* complexes considered by Conradie et al. [44]. Again, the fact that these  $\pi$ -covalency interactions are strong in MAC\*, does not disqualify this ligand, in our estimation, from being considered unambiguously as a redox innocent species. Ligands that expose true redox non-innocence are discussed in Section 3.2.

The arguments of the Ghosh Group contesting the innocence of MAC\* evoke consideration of the oxidation state formalism. For all its obvious limitations, the formalism continues to be a mainstay of classification and intuitive thinking, especially in inorganic chemistry. Of course, given its extraordinary simplicity, we have no right to expect the formalism to work as well as it does in providing a method for systematizing knowledge when dealing with something as complicated as the electronic

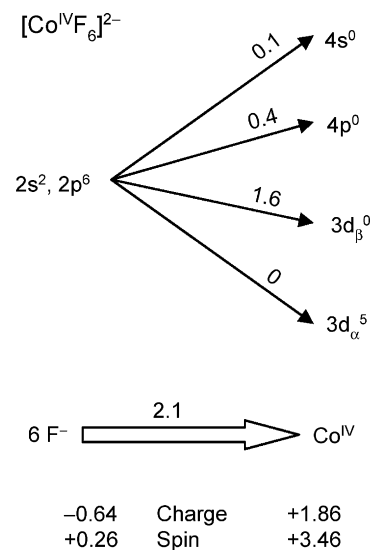


Fig. 7. Mulliken population analysis of the geometry optimized DFT solution for [Co<sup>IV</sup>F<sub>6</sub>]<sup>2−</sup>, obtained with B3LYP/6-311G. The total electron density transferred from the six fluorides to cobalt is indicated above the block arrow. The transfer is decomposed with respect to the accepting metal orbitals by the numbers above the line arrows. The spin and charge densities indicated on the left hand side are for a single fluoride.

<sup>2</sup> The key parameter is the percentage of the total spin density that is located at the ligands, indicated by bold face numerals in Table 6. The doubling of the percentage for the Co complex relative to the Fe species will be explained in the next section.

<sup>3</sup> In spite of a larger pairing energy, the stronger metal–ligand bonds afforded by Co<sup>IV</sup> in [Co<sup>IV</sup>F<sub>6</sub>]<sup>2−</sup> appear to have lowered the energy of the low spin state to below the high spin state. In crystal field theory thinking, this correlates with the expected increase in crystal field splitting that accompanies the increase in oxidation state. We are not aware of experimental evidence in support of this computational result.



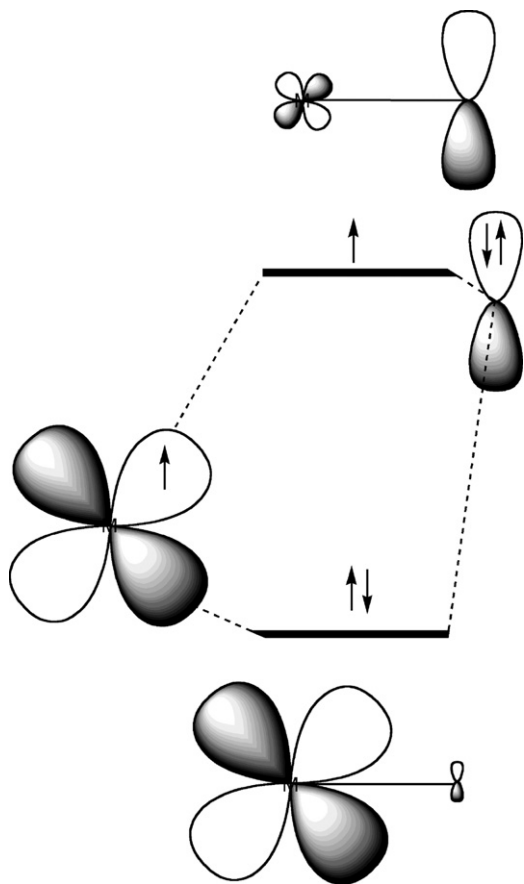


Fig. 8. Orbital diagram illustrating the interaction of a paramagnetic metal ion with a non-innocent ligand. The metal (left) and ligand (right) orbitals retain their character in the interaction because the coupling between them is weak; the orbital size reflects here the weight in the linear combination. As the energy of the metal orbital is below that of the ligand orbital, the  $\beta$  electron of the ligand is transferred to the metal, creating a ligand radical species containing a metal ion with a one-electron reduced formal oxidation state.

structures of transition metal coordination complexes. But in our estimation, it continues to serve the field well, and probably should be retained. If we decide to advance our classification approaches for coordination complexes to incorporate the power of recently acquired computational abilities to better handle the intricacies that are giving the Ghosh Group cause for concern, then we will have to adapt the formalism for all complexes for consistencies sake and jettison the simple formal oxidation states altogether. Oxidation states, if we tried to retain such in this new approach, would no longer have integer values (see Fig. 7).

Neither the Collins nor the Ghosh groups were protagonists when the thinking on the oxidation state formalism was evolving to its current state, which has been in place for a very long time. Were we to attempt to give an account of this history, we would invariably miss many subtleties in accounting for the contributions of so many people to this current state. Of course, the process to attain this state involved much wavering to and fro over the decades while trying to reconcile inconsistencies and acknowledge complexities. From our current vantage point, we can all accept that inorganic chemists have finessed the complexities of the widely varying  $\sigma$ - and  $\pi$ -donation properties of ligands and retained a simple oxidation state formalism instead

of discarding it for a more complicated scheme. While there is always room for debate, we believe that the oxidation states that we have assigned in our papers for  $MQ^1$  systems, often well supported by powerful spectroscopic studies especially in the case of iron, are best left as they stand and that  $[MAC^*]^{4-}$  or  $[Q^1]^{4-}$  should still be considered to provide an excellent innocent coordination environment for attaining complexes of unusual high-oxidation states of middle and later transition metal complexes.

Is there a way to do better than  $[MAC^*]^{4-}$  in designing an innocent ligand system to satisfy the Conradie et al. concerns? Perhaps the best way to significantly neutralize by design  $\pi$ -bonding effects would be to have no lone pairs on the coordinating atoms, but this something that is hard to achieve for high-oxidation states of middle and later transition metals that tend to be powerfully oxidizing, while at the same time it is straight-forward in comparison for early transition metals where the high-oxidation states tend not to be oxidizing. Even if such an approach is effected, with the exception of terminal hydride and perhaps lithide ligands, there remains the potential for  $\pi$ -donor/acceptor interactions arising from the molecular orbitals associated with bonding between the donor atoms and the groups attached to it—Professor Ghosh's concerns may still apply to the resulting complexes. None of this discussion detracts from the important contribution of Professor Ghosh and his collaborators to understanding the electronic structures of  $[Q^1]^{4-}$  complexes by showing so beautifully that they can have significant  $\pi$ -donor properties.

### 3.6. What do the DFT results mean for the broader understanding of the electronic structures of $MQ^1$ systems and for the interpretation of spectroscopic properties?

By studying the table of spin densities in Conradie et al.'s paper [44], the conditions for large  $\pi$  spin densities at the amido nitrogen atoms appear to be that (i) the metal is located inside the  $4N$  plane (planar complex) and that (ii) orbital  $d_{yz}$  contains an unpaired electron—here the  $y$  axis is as shown in Fig. 9 for the idealized  $C_{2v}$  symmetry (planar and octahedral complexes with like axial ligands) or  $C_s$  symmetry (five coordinate or octahedral complexes with unlike axial ligands). Condition (i) ensures favorable overlap between the donor  $N(p\pi)$  and

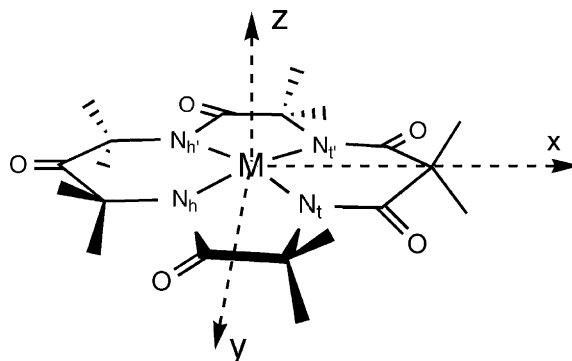


Fig. 9. The axis system used for the discussions of the bonding in  $MQ^1$  complexes (h = head and t = tail).



acceptor  $M(d\pi)$  orbitals. Condition (ii) is rooted in the particular geometry of the quadrangle prescribed by the amidato N atoms. Taking  $[\text{Fe}^{\text{IV}}\text{Q}^1\text{Cl}]^-$  as an example, the lateral distances are, in clockwise order, given as  $N_h-N'_h=2.68\text{ \AA}$ ,  $N'_h-N'_t=2.52\text{ \AA}$ ,  $N'_t-N_t=2.72\text{ \AA}$ , and  $N_t-N_h=2.52\text{ \AA}$ , and correspond to the angles  $N_h\text{--Fe--}N'_h=90^\circ$ ,  $N'_h\text{--Fe--}N'_t=84^\circ$ ,  $N'_t\text{--Fe--}N_t=91^\circ$ , and  $N_t\text{--Fe--}N_h=84^\circ$ , respectively (h = head, t = tail). Since the y axis bisects the sharp bond angles,  $N'_h\text{--M--}N'_t=N_t\text{--M--}N_h<90^\circ$ , the  $d_{yz}$  orbital is “squeezed” between the  $N(p\pi)$  orbitals, leading to a sizable transfer of electron density from, and associated spin density toward the ligand in the case that the receptor orbital is half-filled (see Fig. 6); in addition, the orbital energies appear in the order  $E(d_{xz})<E(d_{yz})$  as a result of the squeezing of  $d_{yz}$  by the  $N(p\pi)$  orbitals and the concomitant relaxation of  $d_{xz}$ . This ordering yields an Aufbau principle according to which  $d_{xz}$  is filled before  $d_{yz}$  (N.B.; the energy gap between  $d_{xz}$  and  $d_{yz}$  is generally not large enough to overcome the pairing energy, so that the electronic configurations are built in the order  $(d_{xz})^1\rightarrow(d_{xz})^1(d_{yz})^1\rightarrow(d_{xz})^2(d_{yz})^1\rightarrow(d_{xz})^2(d_{yz})^2$ ). Including the other  $d$  orbitals, the energy orderings are  $E(d_{x^2-y^2})<E(d_{z^2})<E(d_{xz})<E(d_{yz})<E(d_{xy})$  in four-coordinate complexes (i.e., no axial ligands) and  $E(d_{x^2-y^2})<E(d_{xz})<E(d_{yz})<E(d_{z^2})<E(d_{xy})$  in five- and six-coordinate complexes (with one or two axial ligands). The non-bonding orbital  $d_{x^2-y^2}$  is invariably lowest in energy and the strongly  $\sigma$ -antibonding orbital  $d_{xy}$  is highest and formally unoccupied in all isolated TAML species. The energy of the  $d_{z^2}$  orbital, which is directed along the normal of the  $4N$  plane, is obviously strongly correlated with the number of axial ligands and can move to higher energies than the  $d\pi$  orbitals with added axial ligands. The metal in the four- and six-coordinate complexes is in the  $4N$  plane (cf. Ref. [16]).

Armed with the Aufbau principle and conditions (i) and (ii), the relative magnitudes of the computational results for the  $\pi$  spin densities at the amido-N atoms can be easily predicted:  $[\text{Co}^{\text{IV}}\text{MAC}^*]$  (in-plane) has configuration  $(d_{xy})^2(d_{z^2})^2(d_{xz})^1$  ( $S=1/2$ ) and a small SD,  $[\text{Co}^{\text{IV}}\text{MAC}^*(\text{py})_2]$  (in-plane) has  $(d_{xy})^2(d_{xz})^2(d_{yz})^1$  ( $S=1/2$ ) and a large SD,  $[\text{Fe}^{\text{IV}}\text{MAC}^*(^t\text{BuNC})_2]$  (in-plane) has  $(d_{xy})^2(d_{xz})^1(d_{yz})^1$  ( $S=1$ ) and a large SD,  $[\text{Ni}^{\text{III}}\text{MAC}^*]$  (in-plane) has  $(d_{xy})^2(d_{z^2})^2(d_{xz})^2(d_{yz})^1$  ( $S=1/2$ ) and a large SD, and  $[\text{Fe}^{\text{V}}\text{MAC}^*(\text{O})]^-$  (out-of-plane) has  $(d_{xy})^2(d_{xz})^1$  ( $S=1/2$ ) and a small SD. We pointed out in footnote 2 that the relative spin density at the ligand (i.e., the ligand SD divided by the total SD times 100%) has increased from 29% in  $[\text{Fe}^{\text{IV}}\text{MAC}^*(^t\text{BuNC})_2]$  to 57% in  $[\text{Co}^{\text{IV}}\text{MAC}^*(\text{py})_2]$  (see Table 6). The increase is due to a decrease, from 2 to 1, in the total spin density at nearly unchanged ligand spin density. The invariance of the ligand spin density in these two six-coordinate complexes is found because the same dominating spin polarization mechanism underlies both cases, namely spin polarization induced by an unpaired electron in the dominant  $\pi$ -interacting  $d_{yz}$  orbital (cf. Fig. 6).

Computational studies of complexes with an odd number of electrons in the  $(d_{xz}, d_{yz})$  sub-shell should be conducted with caution. For example, if we impose  $C_s$  symmetry on the complex  $[\text{Fe}^{\text{V}}\text{MAC}^*(\text{O})]^-$ , we obtain an optimized conformation similar to the one reported by Conradie et al. [44], with the unpaired

electron in  $d_{xz}$ . However, symmetry unconstrained optimization of the complex breaks the  $C_s$  symmetry and places the unpaired electron in one of the “diagonal” orbitals,  $d_{x'z}$  or  $d_{y'z}$  ( $x'|N'_h\text{--}N_t$  and  $y'|N_h\text{--}N'_t$ ). The resulting  $C_1$  conformation is  $\sim 2400\text{ cm}^{-1}$  lower in energy than the  $C_s$  conformation. A similar broken symmetry solution for  $[\text{Fe}^{\text{V}}\text{B}^*(\text{O})]^-$  has been reported [47]. The amido nitrogen atoms in the  $C_1$  structure for  $[\text{Fe}^{\text{V}}\text{MAC}^*(\text{O})]^-$  are in a non-planar conformation with unequal “trans” angles  $N'_h\text{--Fe--}N_t=164^\circ$  and  $N_h\text{--Fe--}N'_t=132^\circ$  ( $\approx 150^\circ$  in  $C_s$ ) and distances  $\text{Fe--}N_t\approx\text{Fe--}N'_h\approx 1.92\text{ \AA}$  and  $\text{Fe--}N'_t\approx\text{Fe--}N_h\approx 1.85\text{ \AA}$  ( $\text{Fe--}N\approx 1.90\text{ \AA}$  in  $C_s$ ) for the solution with the unpaired electron in  $d_{x'z}$ .<sup>4</sup> Concomitant with the electronic reorganization there is an increase in the spin densities at the amido nitrogen atoms, +0.026 for  $N_t$  and  $N'_h$  and  $-0.046$  for  $N_h$  and  $N'_t$  ( $\sim -0.01$  in  $C_s$ ). The negative spin densities of the latter atoms are typical for donation into empty  $d$  orbitals ( $d_{y'z}$  and  $d_{xy}$ ) and is caused by the spin polarization of the  $d^\alpha$  and  $d^\beta$  acceptor orbitals under the influence of the exchange field generated by the unpaired electron in  $d_{x'z}$  [47]. But again, while acknowledging the propensity of  $[\text{Q}^1]^{4-}$  to accommodate large spin densities, this ligand remains innocent even as it engages in strongly covalent interactions with high-valent metal ions.

### 3.7. What might the DFT results mean for the reaction chemistry of $\text{MQ}^1$ complexes?

The established nondegeneracy of the  $\text{MQ}^1$   $d_{xz}$  and  $d_{yz}$  orbitals is particularly interesting from a catalyst design point of view. We have for some time, including before the paper in question was published, been continuing the Collins catalyst iterative design strategy with the hitherto unpublished goal of further lifting the degeneracy of  $d_{xz}$  and  $d_{yz}$  to the point of overcoming the electron pairing energy. A coveted goal is to attain by design low spin  $\text{Fe}^{\text{IV}}$  complexes instead of the intermediate and high-spin  $\text{Fe}^{\text{IV}}$ –oxo species found to date, where one can place by design the filled and empty  $\pi^*$  orbitals in known locations in space with respect to the molecular framework. This could have real value in dictating selectivity in the reactions of resulting complexes. For example, if a low spin  $\text{Fe}^{\text{IV}}$ –oxo complex can be attained, then we may be able to achieve an empty  $\text{Fe}^{\text{IV}}$ –oxo  $\pi^*$  LUMO in a prescribed location, specifically  $d_{yz}$  in a species of  $C_s$  symmetry. This may be achievable by clenching more strongly with the  $N(p\pi)$  lone pairs on the  $d_{yz}$  while simultaneously relaxing their grip on  $d_{xz}$ , obviously something one must do through iterative ligand design. Should any of our current strategies succeed, the possibilities for better controlling the electronic structure in the transition states of imaginable energetically gentle oxygen-atom transfer reactions are enticing. Such success would likely increase the value of developing chiral Fe-TAML activators that also include the new features targeted to control the  $\text{Fe}^{\text{IV}}$ –oxo  $\pi^*$  electronic distribution. Of course, this must be done by breaking the mirror plane via changes to selected substituents on the TAML system. The

<sup>4</sup> Results obtained with B3LYP/6-311G for  $\text{MAC}^*$  with hydrogen atoms as tail residues.

same thinking may pertain to the more oxidizing  $\text{Fe}^{\text{V}}$ -oxo complexes already in hand if these strongly oxidizing complexes oxidize appropriate substrates via short range rather than long range processes (electron transfer).

#### 4. Magnetochemistry

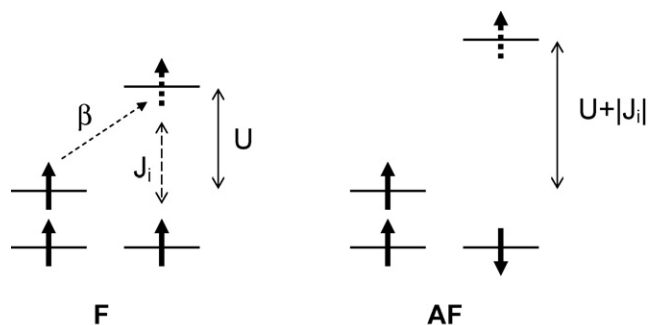
Magnetochemistry is the branch of chemistry that focuses on the relationship between magnetism and molecular structure [48]. Recent interest in this field has been stimulated by the quest for electronic devices that can perform computational and storage operations at a molecular scale [49–51]. These efforts have resulted in the synthesis of an increasing number of polynuclear transition-metal complexes of which the electronic spins,  $S_i$ , of the participating paramagnetic sites are ordered in various patterns. The spin ordering in these systems is generated by exchange interactions, which can often be described by an additive, bilinear spin Hamiltonian,  $\sum_{k<l} J_{kl} \mathbf{S}_k \cdot \mathbf{S}_l$  (the summations are over the paramagnetic sites of the complex) [48]. The exchange interactions are either ferromagnetic ( $J_{kl} < 0$ ) or antiferromagnetic ( $J_{kl} > 0$ ) in nature. A number of coupling mechanisms for explaining the two types of exchange have been described in the literature [52,53]. A profound understanding of the structural and electronic factors that control these mechanisms is essential for the development of a rational approach toward the design of magnetic molecules. As the majority of complexes have antiferromagnetic ( $S = 0$ ) ground states, the pursuit of a rational design strategy is critical for improving the rate of success in attempts to synthesize molecular paramagnetics ( $S > 0$ ). To provide a context for our contributions to this endeavor, we present in the following paragraphs a brief survey of the theory for exchange interactions in molecular complexes.

The constant  $J$  that couples the spins of two co-complexed 3d metal ions is the sum over the contributions pertaining to pairs of 3d orbitals,  $d_i$  and  $d_j$ , located at the interacting metal sites, labeled A and B, respectively:  $J = \sum_{i \in dA} \sum_{j \in dB} j_{ij}$  [53]. The dominant terms in the sum arise from 3d orbital pairs that define pathways for metal-to-metal charge transfer (CT) interactions. Goodenough has pointed out that the sign (ferromagnetic or antiferromagnetic) of the CT contribution to the coupling constant depends on the occupation numbers of the 3d orbitals involved [52]. In the case of a *half-filled–half-filled* orbital pair, in which  $d_i$  and  $d_j$  contain each an unpaired electron, the CT contribution to the coupling is *antiferromagnetic* ( $j_{ij} > 0$ ). These “half–half” pairs prevail in many homovalent binuclear complexes of high-spin ions from the late 3d series,  $d^n \geq 5$ , and result in antiferromagnetic ground states. The CT contributions to  $j_{ij}$  are of the form  $\beta_{ij}^2/U$ , where  $\beta_{ij}$  is a (ligand-mediated) transfer integral connecting orbitals  $d_i$  and  $d_j$ , and  $U$  is the disproportionation energy for the electron transfer  $M_A^{n+} M_B^{n+} \rightarrow M_A^{(n+1)+} M_B^{(n-1)+}$ , which is a large quantity in homovalent complexes (typically 3–10 eV). A comprehensive theoretical analysis of exchange interactions has been given by Anderson [53]. The theory starts from an independent particle model, in which the electrons are described by an orthonormal set of orbitals that are obtained by performing a localization transformation on the molecular

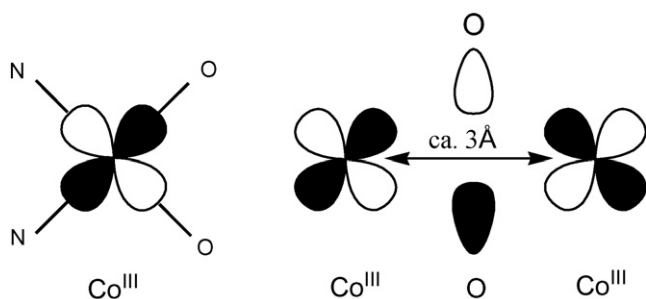
orbitals for the ferromagnetic state. Subsequently,  $J$  is expanded in a many-body perturbational series comprising spin-dependent electron correlation terms. The first-order term is an exchange integral,  $j_{ij,F} \sim -\langle d_i d_j | | d_i d_j \rangle$  ( $d_i$  and  $d_j$  are 3d-type orbitals that are orthogonal to the ligand orbitals), which is ferromagnetic. The second-order contribution includes the aforementioned CT term,  $j_{ij,AF} \sim \beta_{ij}^2/U$ , which is antiferromagnetic. Anderson has argued that  $j_{ij,F}$  and  $j_{ij,AF}$  are the dominant terms in the perturbational series, leading to a powerful formulation according to which  $J$  is the sum of two antagonistic terms,  $J \approx J_F + J_{AF}$ .  $J_{AF}$  is much larger than  $|J_F|$ , unless the transfer matrix elements  $\beta_{ij}$  vanish, either accidentally or for reasons of symmetry, which explains the ubiquity of antiferromagnetic systems. Anderson’s two-term expression for  $J$  has inspired the prevailing design strategy, which aims at configuring molecules, through the choice of ligands and metal ions, in ways that minimize the transfer integrals  $\beta_{ij}$  while maximizing  $\langle d_i d_j | | d_i d_j \rangle$  [48]. A nice example of a detailed analysis, based on Anderson’s superexchange theory, of the magneto-structural correlations in  $\text{Cr}^{\text{III}}$  dimers is presented in Ref. [54]. In the following paragraph, we describe an alternative route toward the control of exchange interactions in multimetallic ions, which is based on CT in *half-filled–empty* orbital pairs.

Goodenough has shown that CT in a *half-filled–empty* orbital pair results in a *ferromagnetic* contribution to the exchange coupling constant [52]. A perturbational treatment gives the expression  $j \sim \beta^2 J_i / U^2$ , where  $\beta$  and  $U$  have similar meanings as above, and  $J_i$  is an *intra-atomic* exchange coupling constant (for details, see Scheme 5 and Refs. [52,55]).

For  $d^n \geq 5$  configurations, empty 3d orbitals are only available if the metal ion is in a state of less than maximum spin.



Scheme 5. The scheme shows an orbital level diagram of a binuclear  $d^2$ – $d^1$  system, illustrating a mechanism of ferromagnetic exchange, proposed by Goodenough [52]. It occurs in the case of electron transfer interaction between a half-filled orbital and an empty orbital.  $\beta$  is a metal-to-metal transfer integral,  $U$  is the energy difference between the donor (solid spin arrow) and acceptor (broken spin arrow) states in the ferromagnetic (F) configuration, and  $J_i$  is an intra-atomic exchange integral ( $J_i < 0$  in  $J_i \mathbf{S}_1 \cdot \mathbf{S}_2$  convention). Intra-atomic exchange is ferromagnetic according to Hund’s rule and raises the energy of the charge transfer configuration in the antiferromagnetic (AF) state relative to the energy of the ferromagnetic state. As a consequence, the transfer interaction lowers the AF ground configuration less in energy than the F configuration, resulting in an effective ferromagnetic exchange coupling ( $J$ ) between the spins at the two metal sites. A second-order perturbation theory treatment of the transfer interaction yields the energies  $-\beta^2/U$  and  $-\beta^2/(U + |J_i|)$  for the F and AF states, respectively. The two expressions yield, after expansion (assuming  $|J_i|/U < 1$ ), a  $J$  coupling on the order of  $-\beta^2 |J_i| / U^2$ .

Scheme 6. Example of exchange pathway between the two  $\text{Co}^{\text{III}}$  centers.

Interestingly, intermediate spin states are the hallmark of the square-planar coordination complexes of  $\text{L}^{\text{I}}$  and  $\text{Q}^{\text{I}}$ . This property follows from the presence of a strong equatorial ligand field, which raises the  $d_{xy}$  level (the  $x$  and  $y$  axes are defined as in Fig. 9) and forces any electron residing in this orbital to pair-off into a lower lying  $d$  orbital. For example, all  $[\text{Co}^{\text{III}}\text{L}^{\text{I}}]^-$  ( $d^6$ ) complexes, for which magnetic data are available, have intermediate ( $S=1$ ) spin states. Under the influence of the strong  $\sigma$ -donor interactions, the empty  $d_{xy}$  orbital at the tetradentate coordination site of  $\text{L}^{\text{I}}$  is significantly delocalized onto the  $2\text{N}/2\text{O}$  atoms, providing an effective communication with the  $d_i$  orbitals of metal ions bound to the exterior, bidentate ( $\text{O}/\text{O}$ ) coordination site of  $\text{L}^{\text{I}}$  (i.e.,  $\beta_{ij}$  is large for  $j=d_{xy}$ ). An example of an exchange pathway involving the empty  $d_{xy}$  orbital is shown in Scheme 6.

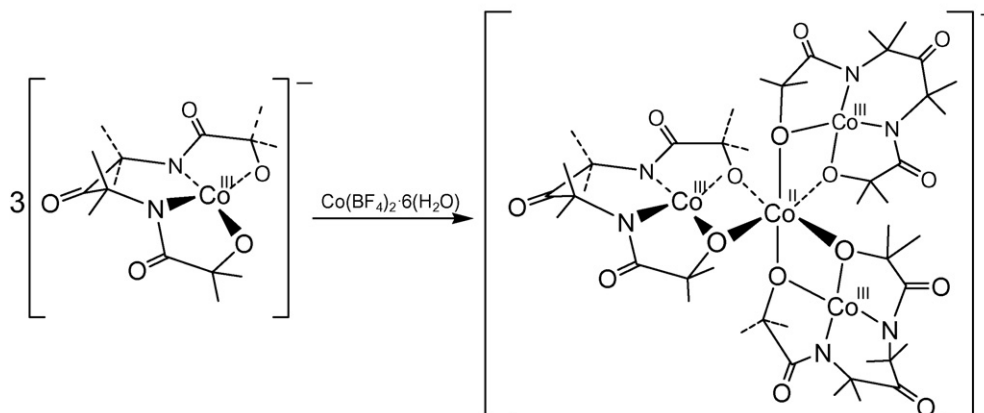
In  $[\{\text{Co}^{\text{III}}(\text{L}^2)\}_3\text{Co}^{\text{II}}]^-$  (Scheme 7), the bidentate coordination sites of the three  $d^6$ ,  $S=1$   $\text{Co}^{\text{III}}(\text{L}^2)$  fragments are occupied by a shared  $\text{Co}^{\text{II}}$  ion ( $d^7$ ,  $S=3/2$ ) [56]. The mixed-valency of the  $\text{Co}^{\text{III}}(\text{L}^2)\text{Co}^{\text{II}}$  motifs is essential for enhancing the Goode-nough term,  $j_{e-h}$ . Given that  $j_{e-h}$  is proportional to  $1/U^2$ , a small value for  $U$  will strengthen  $j_{e-h}$ . Obviously,  $U=0$  for the electron transfer  $M_A^{n+}M_B^{(n+1)+} \rightarrow M_A^{(n+1)+}M_B^{n+}$  in mixed-valence dimers with identical coordination sites. In the  $U=0$  case, the expression for  $j_{e-h}$  and the bilinear spin Hamiltonian it represents are not applicable anymore and should be replaced by the effective operator for double exchange [57]. However, the  $U$  in  $[\{\text{Co}^{\text{III}}(\text{L}^2)\}_3\text{Co}^{\text{II}}]^-$  is a nonzero quantity because the cobalt ions are placed in different coordination spheres ( $\text{Co}^{\text{II}}$  has an octahedral  $6\text{O}$  coordination and  $\text{Co}^{\text{III}}$  has a square-planar  $2\text{N}/2\text{O}$

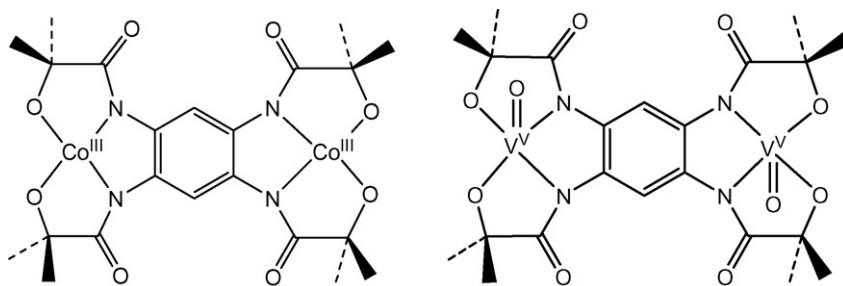
coordination). As  $U$  is now a ligand-field splitting and not a disproportionation energy, its value is most likely smaller than in homo-valent species (see above).

In summary, complex  $[\{\text{Co}^{\text{III}}(\text{L}^2)\}_3\text{Co}^{\text{II}}]^-$  presents a set of favorable conditions for ferromagnetic coupling between the central  $\text{Co}^{\text{II}}$  and the terminal  $\text{Co}^{\text{III}}$  sites because: (i) the  $\text{Co}^{\text{III}}$  ions have an empty  $d$  orbital, (ii) there are large transfer matrix elements connecting these empty  $d$  orbitals with the half-filled orbitals at  $\text{Co}^{\text{II}}$ , and (iii)  $U$  is relatively small due to the mixed-valency of the multinuclear ion.

Since the complex lacks effective exchange pathways between the  $\text{Co}^{\text{III}}$  sites, the couplings between them can be assumed to be negligibly small. The magnetic state of the complex is thus determined by the ferromagnetic exchange couplings between the central  $\text{Co}^{\text{II}}$  and the peripheral  $\text{Co}^{\text{III}}$  ions. These interactions it was thought would align the  $S=1$  spins of the three  $\text{Co}^{\text{III}}$  ions parallel to the  $S=3/2$  spin of the  $\text{Co}^{\text{II}}$  and result in a ground state with total spin  $S=9/2$ . This prediction was tested by variable-temperature EPR and magnetic susceptibility measurements on  $[\{\text{Co}^{\text{III}}(\text{L}^2)\}_3\text{Co}^{\text{II}}][\text{PPh}_4]$ . The EPR shows an axial signal with  $g_{\perp}=9.65$ , which is close to the  $g_{\perp}\approx 10$  predicted for the  $M_S=\pm 1/2$  doublet of the anticipated ground-state spin  $S=9/2$  multiplet. The curve of  $\mu_{\text{eff}}$  versus temperature has a maximum of  $9.7\mu_B$  at 40 K, which is close to the spin-only value  $9.95\mu_B$  for  $S=9/2$ . The value of  $\mu_{\text{eff}}$  decreases when the temperature is raised above 40 K due to population of excited states with lower spin. The temperature dependence of  $\mu_{\text{eff}}$  has been analyzed with a theoretical model that accounts for exchange and spin-orbit coupling, which both have an important impact on the energy levels of the complex [43]. The analysis yields a ferromagnetic coupling,  $J(\text{Co}^{\text{II}}-\text{Co}^{\text{III}})=-22\pm 5\text{ cm}^{-1}$ .

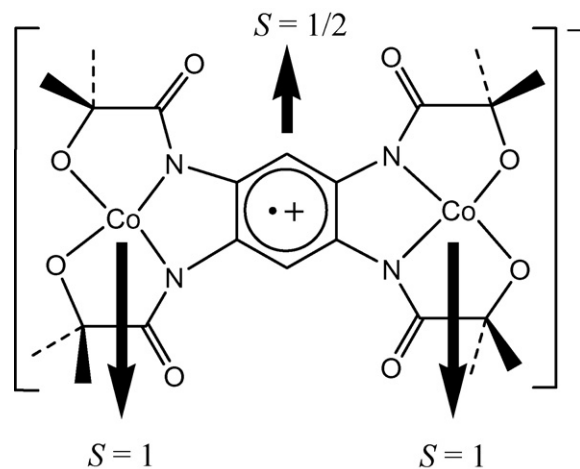
High-spin multinuclear ions with axial zero-field splittings,  $DS_z^2$ , have for  $D<0$  a twofold degenerate ground doublet,  $M_S=\pm S$ . Since for large values of  $S$  the lifetimes of the two states can be considerable, multinuclear ions have been proposed as data storage devices [50,51,58]. However, the positive zero-field splitting prevailing in  $[\{\text{Co}^{\text{III}}(\text{L}^2)\}_3\text{Co}^{\text{II}}]^-$  makes this multinuclear ion unsuitable for storage purposes and the group was turning its attention in the mid-1990s to finding more desirable multinuclear ions for exploration in such application areas.

Scheme 7. Synthesis of the tetranuclear ion  $[\{\text{Co}^{\text{III}}(\text{L}^2)\}_3\text{Co}^{\text{II}}]^-$ .

Fig. 10. Structures of  $[(\text{Co}^{\text{III}})_2(\text{L}')^{2-}]$  and  $[(\text{V}^{\text{VO}})_2(\text{L}')^{2-}]$  dimers.

The exchange interactions considered thus far are transmitted through *diamagnetic* ligand bridges and are often referred to as ‘indirect’ or ‘super’ exchange [53]. In this paragraph, we consider spin ordering induced by *paramagnetic* ligands, which can be obtained by oxidizing non-innocent ligands, such as the phenyl-centered ligand  $\text{L}'$ . Such species came under design as beginning efforts aimed at extending the local control an  $[\{\text{M}_a(\text{L}^2)\}_3\text{M}_b]^{n-}$  ion to larger multimetallic multinuclear ions and eventually to crystals. Two precursor  $\text{M}_2\text{L}'$  complexes were characterized by X-ray crystallography, namely,  $[(\text{V}^{\text{VO}})_2\text{L}']^{2-}$  and  $[\text{Co}_2^{\text{III}}\text{L}']^{2-}$  (Fig. 10 and Table 7) [20,43].

The cyclic voltammogram of  $[(\text{V}^{\text{VO}})_2\text{L}']^{2-}$  showed a  $1\text{e}^-$ -oxidation at  $E^\circ = 0.350\text{ V}$  (in  $[\text{Bu}_4\text{N}]^+[\text{PF}_6]^-/\text{CH}_3\text{CN}$  versus SSCE) [59]. The oxidation product has been isolated and assigned to a radical species,  $\text{L}'\cdot$ , as the  $d^0$  configuration of  $\text{V}^{\text{V}}$  precludes metal-based oxidation. This assignment was confirmed by EPR measurements, which revealed a narrow, isotropic  $g = 2$  signal typical for organic radicals. The magnetic susceptibility data for  $[\text{Co}_2^{\text{III}}\text{L}']^{2-}$  revealed the presence of two weakly interacting  $S = 1$  sites,  $J(\text{Co}^{\text{III}}-\text{Co}^{\text{III}}) \approx 0$ , indicating that the central  $[\text{C}_6\text{H}_2\text{N}_4]^{4-}$  moiety of  $\text{L}'$  provides an inefficient superexchange pathway between these metal ions.  $[\text{Co}_2^{\text{III}}\text{L}']^{2-}$  undergoes electrochemical oxidation at  $E^\circ = 0.290\text{ V}$  (versus SSCE). The oxidation potential is close to the potential for the vanadyl complex, which suggests that the oxidation of  $[\text{Co}_2^{\text{III}}\text{L}']^{2-}$  is also ligand based. Since the phenyl group is the only site for a ligand-based oxidation,  $[\text{Co}_2\text{L}']^{2-}$  must contain two  $\text{Co}^{\text{III}}$  sites linked by a radical:  $[\text{Co}^{\text{III}}\text{L}'\cdot\text{Co}^{\text{III}}]^-$ . The radical has a dramatic effect on the magnetic properties of the cobalt complex. Taking into consideration that the metals and the radical are neighbors and assuming the common ‘half-half’ type of exchange, the coupling constants  $J(\text{Co}^{\text{III}}-\text{L}'\cdot)$  between the radical and the two  $\text{Co}^{\text{III}}$  ions should be strong and anti-ferromagnetic. The couplings align the  $\text{Co}^{\text{III}}$  spins antiparallel to the radical spin, leading to parallel ordering of the  $\text{Co}^{\text{III}}$  spins and a ground state with total spin  $S = 3/2$  (Scheme 8).

Scheme 8. Spin alignment of the  $\text{Co}^{\text{III}}$  centers and ligand radical cation in the  $S = 3/2$  system.

The ferrimagnetic  $[\text{Co}_2^{\text{III}}\text{L}'\cdot]$  units can subsequently be used as linkers for inducing parallel alignment of the spins of the paramagnetic centers,  $\text{M}_b$ , in a hypothetical complex such as  $\{[\text{Co}_2^{\text{III}}\text{L}'\cdot]_2\text{M}_b[\text{Co}_2^{\text{III}}\text{L}'\cdot]\text{M}_b[\text{Co}_2^{\text{III}}\text{L}']_2\}^{n-}$ , which is beginning to look like the type of multinuclear ion from which one might extend the structure to build a magnetic crystal.

The spin functions for the ground and excited states of  $[\text{Co}_2^{\text{III}}\text{L}'\cdot]$  are eigenstates of the Hamiltonian  $J(S_A + S_B) \cdot S_R$ , where  $J = J(\text{Co}^{\text{III}}-\text{L}'\cdot)$ ,  $S_A = S_B = 1$  are the spins for the cobalt atoms,  $S_R = 1/2$  is the radical spin, and the coupling constant between the cobalt ions is assumed to vanish as in  $[\text{Co}_2^{\text{III}}\text{L}']^{2-}$ . The spin states can be formulated as  $|(S_{AB}, S_R)S\rangle$ , where the coupled spin  $S_{AB}$  of the two cobalt centers can take the values 0, 1, 2, and the total spin  $S$  is confined by the triangular condition  $|S_{AB} - 1/2| \leq S \leq S_{AB} + 1/2$ . The energies are given by  $E(S, S_{AB}) = 1/2 J[S(S+1) - S_{AB}(S_{AB}+1) - 3/4]$ . The ground state,  $|(2, 1/2)S = 3/2\rangle$ , is supported by EPR measurements

Table 7

Selected X-ray/DFT bond lengths (Å) and Mulliken spin density values of cobalt and vanadium dimers

Complex	M–O	M–N	C5–C6	C6–C7	Mulliken spin densities			
					Co	C5	C6	C7
$[(\text{Co}^{\text{III}})_2(\text{L}')^{2-}]$	1.796(4)/1.820	1.821(4)/1.838	1.415(4)/1.423	1.385(4)/1.403	−/1.760	−/0.002	−/0.002	−/0.013
$[(\text{Co}^{\text{III}})_2(\text{L}'\cdot)^-]$	−/1.802	−/1.843	−/1.462	−/1.400	−/1.725	−/−0.163	−/−0.163	−/0.106
$[(\text{V}^{\text{VO}})_2(\text{L}')^{2-}]$	1.803(4)/1.803	2.006(4)/2.039	1.400(4)/1.457	1.391(4)/1.401				



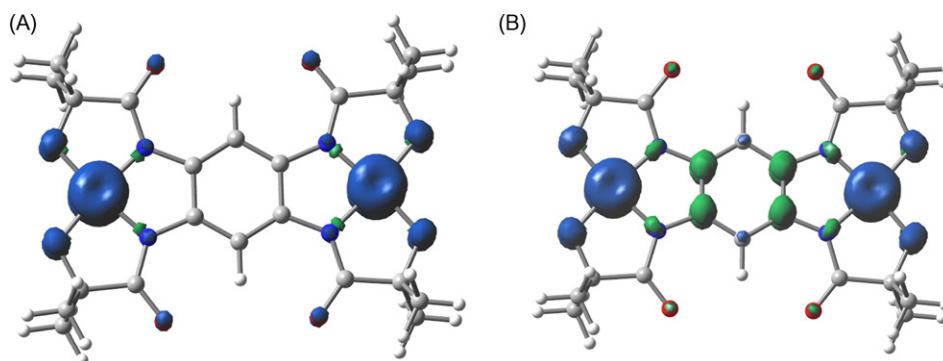


Fig. 11. DFT spin density mappings: (A)  $[(\text{Co}^{\text{III}})_2(\text{L}')_2]^{2-}$  ( $S=2$ ) and (B)  $[(\text{Co}^{\text{III}})_2(\text{L}'\bullet\bullet)]^-$  ( $S=3/2$ ). Positive and negative spin densities are in blue and green, respectively. (For interpretation of the references to color in this figure legend, the reader is referred to the web version of the article.)

of  $[\text{PPh}_4][\text{Co}_2\text{L}'\bullet\bullet]$  in frozen  $\text{CH}_2\text{Cl}_2$  solution, which show a rhombic signal with effective  $g$  factors  $g_1 = 5.63$ ,  $g_2 = 4.01$ , and  $g_3 = 1.98$ . The average  $(g_1 + g_2)/2 = 4.8$  is larger than the spin-only value 4 for the ground doublet  $|S=3/2, M=\pm 1/2\rangle$  due to orbital contributions to the intrinsic  $g$  values which arise from spin–orbit coupling. The three-spin formulation of  $[\text{Co}_2\text{L}'\bullet\bullet]^-$  implies that the spin ladder includes states with total spin  $S=1/2$ ,  $3/2$ , and  $5/2$ . Of the three states, the  $S=5/2$  state is highest in energy and the Boltzmann population of this state should give rise to an *increase* of  $\mu_{\text{eff}}$  upon raising the temperature. The  $S=5/2$  state is absent in the two-spin formulation pertinent to the event of metal-based oxidation,  $[\text{Co}^{\text{III}}\text{L}'/\text{Co}^{\text{IV}}]^-$ . In this case the spin states are  $|S_A=1, S_B=1/2\rangle S\rangle$  and there is, in addition to the  $S=3/2$  ground state, only an  $S=1/2$  excited state. In the two-spin scenario, the Boltzmann population of the  $S=1/2$  state should increase upon raising the temperature and result in a *decrease* of  $\mu_{\text{eff}}$ . These predictions were tested by performing magnetic susceptibility measurements on a powder sample of  $[\text{Co}_2\text{L}'][\text{PPh}_4]$  [59]. The value of  $\mu_{\text{eff}}$  increases with increasing temperature as predicted by three-spin model. A spin-Hamiltonian fit of the  $\mu_{\text{eff}}$  versus  $T$  plot yields, as predicted, a large antiferromagnetic exchange coupling constant,

$J(\text{Co}^{\text{III}}-\text{L}'\bullet\bullet) \approx 75 \text{ cm}^{-1}$ , which implies an ferrimagnetic alignment of the three spins. The radical nature of the bridging ligand in  $[\text{Co}_2\text{L}'\bullet\bullet]^-$  is supported by DFT calculations. The spin density plot obtained for the  $M_S = 3/2$  state shows that on oxidation of  $[\text{Co}_2^{\text{III}}\text{L}']^{2-}$  a  $\pi$  electron is removed from the bridge (Fig. 11). In conclusion, a comparison of the magnetic data for  $[\text{Co}_2\text{L}']^{2-}$  and  $[\text{Co}_2\text{L}'\bullet\bullet]^-$  shows that the oxidation of a weak superexchange bridge to a radical may turn it into a potent enforcer of ferromagnetic spin ordering. The complex  $[\text{Co}_2\text{L}'\bullet\bullet]^-$  is, by no means, the only example of a polynuclear radical species. Other examples of these interesting systems have recently been reported by Wieghardt and coworkers [60–62].

As work continued to obtain a network solid based on  $[\text{Co}_2\text{L}']^{2-}$  or related dimers, we began considering a priori the types of network solids that might be achievable. Tetranuclear  $[\{\text{Co}^{\text{III}}(\text{L}^2)\}_3\text{Co}^{\text{II}}]^-$ , the basic model from which we hoped to design network crystals, belongs to the  $D_3$  point group. This point group does not contain an improper rotation axis, therefore,  $D_3$  ions are chiral. Moreover, one can realize that the species is propeller-like in structure (Fig. 12). If adjacent  $M_b$  sites in a network solid have alternating handedness, then a planar sheet structure is obtained (Fig. 13). In such a crystal, anisotropic

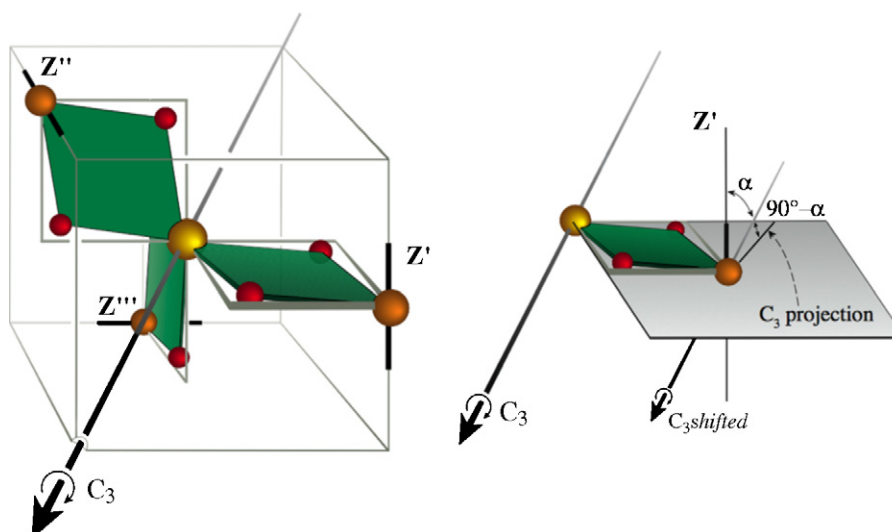


Fig. 12. (Left) Schematic representation of geometry of the tetranuclear complex showing the orthogonality of the “propeller blades” represented by the bridging O-atoms and the  $\text{Co}^{\text{III}}$  centers. (Right) A representation of one propeller blade showing important angles. The angle  $90^\circ - \alpha$  is designated  $\rho$ .



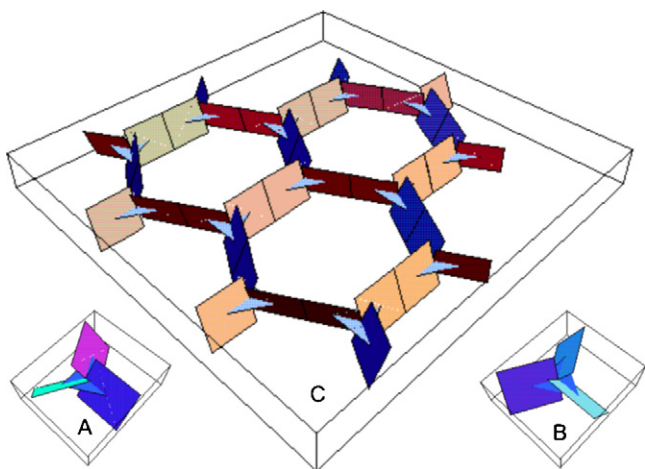


Fig. 13. (A) Counterclockwise molecular propeller. (B) Clockwise molecular propeller. (C) Planar sheet structure with alternating chirality for adjacent  $M_b$  ions.

effects of pressure on the magnetic properties could be imagined. Network solids comprised of interconnected helices result when adjacent  $D_3$  sites retain the same handedness and examples were being described in the literature at the time [20]. It was reasoned that the  $M_b$  ion might be the focus of a significant magneto-structural relationship. Specifically, the structures and exchange interactions of network solids should be dependent on the  $M_b$ -related angle,  $90^\circ - \alpha$ , designated  $\rho$  (Fig. 12). The angle  $\rho$  is the angle the propeller blades make with the  $C_3$  axis or more generally with the local  $M_b$  based  $z$  axis; we called  $\rho$  “the pitch angle”. For certain  $M_b$  ions, e.g., high-spin  $Fe^{III}$  and high-spin  $Mn^{II}$ , we considered it likely that the  $\rho$  of a  $[Co^{III}(L^2)]_3M_b]^{m-}$ -like complex would be free to move over a considerable range. In these cases, there would be no crystal field stabilization to require the  $M_b$ -ligand bonding to be strongly directional. The  $M_b$  contribution to controlling the structure should be valence shell electron pair repulsion-like. Other ions with weak crystal field stabilizations such as intermediate spin  $Co^{II}$  should also possess a flexible  $\rho$ . Thus, for certain ions, the pitch angle of the propeller blades should be free to move in solution primarily within the limits of steric interactions. In the solid state, we envisioned the size of  $\rho$  would be determined by local steric and crystal packing forces including counterion effects, periodicity requirements and steric forces. In  $[Co^{III}(L^2)]_3Co^{II}]^-$ ,  $\rho$  was determined to be  $35.3^\circ$ . And in this compound, steric reasons for preventing formation of the  $D_{3h}$  structure with  $\rho = 0^\circ$  were not evident such that if one assumed a sufficiently weak directionality of the  $Co^{II}-O$  bonding, all angles between  $0^\circ$  and the experimentally observed  $35.3^\circ$  could be accessible in solution.

While we never got to investigate the possibility for reasons described in the introduction and repeated shortly below, a system with ferric ion as  $M_b$  was particularly interesting because if a network solid with  $[Co_2L']^{2-}$  could be crystallized, its overall charge would be neutral and it would possibly be easy to crystallize as a result. We reasoned that following the diffusion of an oxidant such as a halogen into the crystal lattice to convert the  $[Co_2L']^{2-}$  to  $[Co_2L'\bullet]^-$ , the magnetic effects would be able to be turned on progressively.

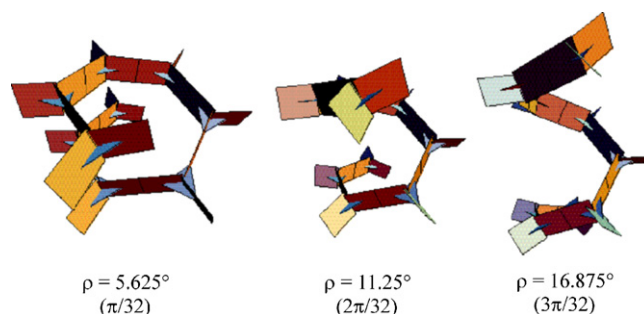


Fig. 14. Diagram showing significant dependence of the helical extension on  $\rho$ .

Many interesting consequences of a variable  $\rho$  are conceivable. Solution EPR resonances could be broadened; variable  $\rho$ -induced broadenings could be present in the EPR spectrum of  $[Co^{III}(L^2)]_3Co^{II}]^-$ . For a growing helix based upon a repeating unit of, for example,  $[Co_2^{III}L']\{Co^{III}(L^2)\}Fe^{III}]$ , the linear growth rate per multimetallic ion would be  $\rho$  dependent. This dependence is schematically depicted in Fig. 14 for the pitch angle range of  $\pi/32$ – $3\pi/32$ . It is also likely that the exchange coupling would be  $\rho$  sensitive. Thus, it seemed reasonable to propose that the magnetic properties of macromolecular solids of the type that we and others were targeting at the time would be strongly pressure dependent [20]. The dependence should be found for networks based on helices, chains or sheets and should also exist for solids based on smaller oligomers such as rings. These ideas called for many novel investigations.

It was further noted at the time [20] that two other significant molecular parameters are constant for a given building unit;  $L$ , the distance between two consecutive  $M_b$  ions, and  $2\tau$ , the angle at a given  $M_b$  ion spanned by the two adjacent  $M_b$  ions; for a  $D_3$  multimetallic ion,  $\tau$  is  $60^\circ$ . Theoretical structures composed of the molecular units defined by the local values of  $\rho$ ,  $\tau$ , and  $L$  can be generated by a sequence of rotations, translations or reflections performed on a single molecular unit. For instance, a sequence of rotations and translations performed on a single repeat unit of composition  $[Co_2^{III}L']\{Co^{III}(\kappa^4-1)\}Co^{II}]$  (also of neutral charge) yields the helix of Fig. 15A, where we have found a mathematical treatment to be helpful in appreciating the various allowed structures and their inter-relationships especially with respect to the key molecular variable  $\rho$ . The relevant molecular and helical parameters were presented in Fig. 15B [20] which depicts a single  $Co^{II}-Co^{II}$  step in the context of the cylinder around which an ideal helix would wind; this helix would pass through each  $Co^{II}$  ion. The structural properties of the helix can be expressed as functions of the molecular parameters  $\rho$ ,  $L$  and  $\tau$ . Important additional parameters are:  $h_z$ , the  $z$  axis of the cylinder;  $w$ , the radius of the cylinder;  $l$ , the projection of  $L$  onto the  $(h_x, h_y)$  plane;  $\theta$  an angle analogous to the variable  $\Theta$  from the helical function,  $z = k\Theta$ ;  $t$ , the projection of  $L$  onto  $h_z$ ;  $\gamma$ , the angle subtended between  $L$  and  $l$ ; and  $f$ , the lines joining the origin of each  $Co^{II}$ -containing circular section of the cylinder to each of the immediate  $Co^{II}$  neighbors.

While  $\rho$  is the key molecular variable for controlling the helical extension (Fig. 14),  $\gamma$  employed within the helical coordinate system  $(x_1, y_1, z_1)$  is the key variable for controlling the helical



gral component of the genesis of an oxidatively resistant set of ligands that are capable of stabilizing high-oxidation state middle and later transition-metal complexes and delivering potent peroxidase mimics. The ligand systems have provided a stimulating landscape on which to explore many aspects of inorganic chemistry emphasizing the interplay of design and measurement to achieve targeted properties. Some of the more intriguing features suggest technologically useful products and processes beyond those now well-established for Fe-TAML activators. The ligand systems of PAC ( $H_4L$  and  $H_4P$ ) were redesigned into the macrocyclic systems of TAMLs ( $H_4Q$  and  $H_4T$ ) in the pursuit of much more advantageous coordination environments for attaining our most important strategic goal, namely the design of effective small molecule oxidation catalysis to reproduce the chemistry of oxygenase and peroxidase enzymes. Though the complexes described here have revealed a wide spectrum of intriguing properties, none of these species have turned out to be great oxidation catalysts. While each design step was taken with the hope that it would lead to effective oxidation catalysts, the frustrations of inadequate catalysts found for so many cycles of the design loop was by no means fatally discouraging. In hindsight, we can recognize that each step was simply part of what turned out to be a necessary 15-year design evolution to the successful Fe-TAML oxidation catalysts. With each new iterated ligand, iron was the first element to have its coordination chemistry explored. As it turned out, much of the exploratory chemistry had to be performed on osmium (not described here) and non-iron first row metals (reviewed here) because the iron coordination chemistry would not give mononuclear species (each such disappointing discovery was not reported by us). The solid background described here cleared the way for developing the chemistry of iron, nature's primary transition metal for oxidation catalysis, when we reached the TAML ligand systems. TAML systems were first reported in 1990 to have appropriate electronic and coordinative properties to give the much-desired iron-mononuclear species [63]. However, it then took till 1995 for us to convincingly achieve Fe-TAML systems with sufficient resistance to oxidative and hydrolytic decay and show them to be long enough lived to be useful. The now-familiar catalysis story involving extremely useful peroxidase and intriguing oxygenase mimics evolved from there [4].

## References

- [1] H.B. Dunford, Heme Peroxidases, Wiley-VC, 1999.
- [2] I. Bertini, H.B. Gray, S.J. Lippard, J.S. Valentine, Bioinorganic Chemistry, Univ. Sci. Books, 1994.
- [3] T.J. Collins, S.W. Gordon-Wylie, M.J. Bartos, C.P. Horwitz, C.G. Woomer, S.A. Williams, R.E. Patterson, L.D. Vuocolo, S.A. Paterno, S.A. Strazisar, D.K. Peraino, C.A. Dudash, Green Chem. (1998) 46.
- [4] T.J. Collins, C. Walter, Sci. Am. 294 (2006) 83.
- [5] T.J. Collins, Acc. Chem. Res. 27 (1994) 279.
- [6] T.J. Collins, Acc. Chem. Res. 35 (2002) 782.
- [7] C.P. Horwitz, D.R. Fooksman, L.D. Vuocolo, S.W. Gordon-Wylie, N.J. Cox, T.J. Collins, J. Am. Chem. Soc. 120 (1998) 4867.
- [8] M.J. Bartos, S.W. Gordon-Wylie, B.G. Fox, L. James Wright, S.T. Weintraub, K.E. Kauffmann, E. Münck, K.L. Kostka, E.S. Uffelman, C.E.F. Rickard, K.R. Noon, T.J. Collins, Coord. Chem. Rev. 174 (1998) 361.
- [9] A. Ghosh, F. Tiago de Oliveira, T. Yano, T. Nishioka, E.S. Beach, I. Kinoshita, E. Münck, A.D. Ryabov, C.P. Horwitz, T.J. Collins, J. Am. Chem. Soc. 127 (2005) 2505.
- [10] C.P. Horwitz, T.J. Collins, J. Spatz, H.J. Smith, L.J. Wright, T.R. Stuthridge, K.G. Wingate, K. McGrouther, ACS Symp. Ser. 921 (2006) 156.
- [11] D. Banerjee, A.L. Markley, T. Yano, A. Ghosh, P.B. Berget, E.G. Minkley Jr., S.K. Khetan, T.J. Collins, Angew. Chem., Intl. Ed. 45 (2006) 3974.
- [12] S.S. Gupta, M. Stadler, C.A. Noser, A. Ghosh, B. Steinhoff, D. Lenoir, C.P. Horwitz, K.-W. Schramm, T.J. Collins, Science 296 (2002) 326.
- [13] S. Mondal, Y. Hangan-Balkir, L. Alexandrova, D. Link, B. Howard, P. Zandhuis, A. Cugini, C.P. Horwitz, T.J. Collins, Catal. Today 116 (2006) 554.
- [14] A. Chanda, S. Khetan, D. Banerjee, A. Ghosh, T.J. Collins, J. Am. Chem. Soc. 128 (2006).
- [15] A. Ghosh, A.D. Ryabov, S.M. Mayer, D.C. Horner, D.E. Prasuhn Jr., S. Sen Gupta, L. Vuocolo, C. Culver, M.P. Hendrich, C.E.F. Rickard, R.E. Norman, C.P. Horwitz, T.J. Collins, J. Am. Chem. Soc. 125 (2003) 12378.
- [16] A. Chanda, D.-L. Popescu, F. Tiago de Oliveira, E.L. Bominaar, A.D. Ryabov, E. Münck, T.J. Collins, J. Inorg. Biochem. 100 (2006) 606.
- [17] M.J. Frisch, G.W. Trucks, H.B. Schlegel, G.E. Scuseria, M.A. Robb, J.R. Cheeseman, J.J.A. Montgomery, T. Vreven, K.N. Kudin, J.C. Burant, J.M. Millam, S.S. Iyengar, J. Tomasi, V. Barone, B. Mennucci, M. Cossi, G. Scalmani, N. Rega, G.A. Petersson, H. Nakatsuji, M. Hada, M. Ehara, K. Toyota, R. Fukuda, J. Hasegawa, M. Ishida, T. Nakajima, Y. Honda, O. Kitao, H. Nakai, M. Klene, X. Li, J.E. Knox, H.P. Hratchian, J.B. Cross, C. Adamo, J. Jaramillo, R. Gomperts, R.E. Stratmann, O. Yazyev, A.J. Austin, R. Cammi, C. Pomelli, J.W. Ochterski, P.Y. Ayala, K. Morokuma, G.A. Voth, P. Salvador, J.J. Dannenberg, V.G. Zakrzewski, S. Dapprich, A.D. Daniels, M.C. Strain, O. Farkas, D.K. Malick, A.D. Rabuck, K. Raghavachari, J.B. Foresman, J.V. Ortiz, Q. Cui, A.G. Baboul, S. Clifford, J. Cioslowski, B.B. Stefanov, G. Liu, A. Liashenko, P. Piskorz, I. Komaromi, R.L. Martin, D.J. Fox, T. Keith, M.A. Al-Laham, C.Y. Peng, A. Nanayakkara, M. Challacombe, P.M.W. Gill, B. Johnson, W. Chen, M.W. Wong, C. Gonzalez, J.A. Pople, Gaussian 03, Gaussian Inc., Pittsburgh, PA, 2003.
- [18] F.C. Anson, J.A. Christie, T.J. Collins, R.J. Coots, T.T. Furutani, S.L. Gipson, J.T. Keech, T.E. Krafft, B.D. Santarsiero, G.H. Spies, J. Am. Chem. Soc. 106 (1984) 4460.
- [19] A.B.P. Lever, Inorg. Chem. 29 (1990) 1271.
- [20] S.W. Gordon-Wylie, B.L. Claus, C.P. Horwitz, Y. Leychikis, J.M. Workman, A.J. Marzec, G.R. Clark, C.E.F. Rickard, B.J. Conklin, S. Sellers, G.T. Yee, T.J. Collins, Chem. Eur. J. 4 (1998) 2173.
- [21] T.J. Collins, R.D. Powell, C. Slebodnick, E.S. Uffelman, J. Am. Chem. Soc. 113 (1991) 8419.
- [22] T.J. Collins, K.L. Kostka, E.S. Uffelman, T.L. Weinberger, Inorg. Chem. 30 (1991) 4204.
- [23] T.J. Collins, S.W. Gordon-Wylie, J. Am. Chem. Soc. 111 (1989) 4511.
- [24] W.A. Nugent, J.M. Mayer, Metal-Ligand Multiple Bonds: The Chemistry of Transition Metal Complexes Containing Oxo, Nitrido, Imido, Alkylidene, or Alkylidyne Ligands. Wiley Interscience, 1988.
- [25] M. Bera, K. Biradha, R. Ray, Inorg. Chim. Acta 174 (1990) 57.
- [26] J.T. Groves, J. Lee, S.S. Marla, J. Am. Chem. Soc. 119 (1997) 6269.
- [27] M. Palucki, N.S. Finney, P.J. Pospisil, M.L. Güler, T. Ishida, E.N. Jacobsen, J. Am. Chem. Soc. 120 (1998) 948.
- [28] T.J. Collins, T.G. Richmond, B.D. Santarsiero, B.G.R.T. Treco, J. Am. Chem. Soc. 108 (1986) 2088.
- [29] C.G. Miller, S.W. Gordon-Wylie, C.P. Horwitz, S.A. Strazisar, D.K. Peraino, G.R. Clark, S.T. Weintraub, T.J. Collins, J. Am. Chem. Soc. 120 (1998) 11540.
- [30] F.C. Anson, T.J. Collins, R.J. Coots, S.L. Gipson, T.G. Richmond, J. Am. Chem. Soc. 106 (1984) 5037.
- [31] T.J. Collins, J.M. Workman, Angew. Chem., Intl. Ed. 101 (1989) 924.
- [32] J.C. Brewer, T.J. Collins, M.R. Smith, B.D. Santarsiero, J. Am. Chem. Soc. 110 (1988) 423.
- [33] W.P. Schaefer, B.T. Huie, M.K. Kurilla, S.E. Ealick, Inorg. Chem. 19 (1980) 340.
- [34] T.J. Collins, S. Ozaki, T.G. Richmond, J. Chem. Soc., Chem. Commun. (1987) 803.

- [35] S. Ozaki, H. Mimura, N. Yasuhara, M. Masui, Y. Yamagata, K. Tomita, T.J. Collins, *J. Chem. Soc. Perkin Trans. 2* (1990) 353.
- [36] T.J. Collins, E.S. Uffelman, *Angew. Chem., Intl. Ed.* 101 (1989) 1552.
- [37] T.J. Collins, T.R. Nichols, E.S. Uffelman, *J. Am. Chem. Soc.* 113 (1991) 4708.
- [38] T.J. Collins, C. Slebodnick, E.S. Uffelman, *Inorg. Chem.* 29 (1990) 3433.
- [39] C.P. Horwitz, S.W. Gordon-Wylie, Y. Leychkis, D.M. Flynn, S.T. Weintraub, G.R. Clark, T.J. Collins, *J. Phys. Chem. B* 105 (2001) 8821.
- [40] R.E. Patterson, S.W. Gordon-Wylie, C.G. Woomer, R.E. Norman, S.T. Weintraub, C.P. Horwitz, T.J. Collins, *Inorg. Chem.* 37 (1998) 4748.
- [41] F.C. Anson, T.J. Collins, T.G. Richmond, B.D. Santarsiero, J.E. Toth, B.G.R.T. Treco, *J. Am. Chem. Soc.* 109 (1987) 2974.
- [42] L.L. Diaddario, W.R. Robinson, D.W. Margerum, *Inorg. Chem.* 22 (1983) 1021.
- [43] T.J. Collins, S.W. Gordon-Wylie, E.L. Bominaar, C.P. Horwitz, G. Yee, in: E.O. Kahn (Ed.), *NATO ASI Series, Series C: Mathematical and Physical Sciences*, vol. 484, Dordrecht, 1996, p. 509.
- [44] M.M. Conradie, J. Conradie, A. Ghosh, *J. Inorg. Biochem.* 100 (2006) 620.
- [45] F.A. Cotton, M.D. Meyers, *J. Am. Chem. Soc.* 82 (1960) 5023.
- [46] B.N. Figgis, *Nature* 182 (1958) 1568.
- [47] F. Tiago de Oliveira, A. Chanda, D. Banerjee, X. Shan, S. Mandal, L. Que Jr., E.L. Bominaar, E. Münck, T.J. Collins, *Science* 315 (2007) 835.
- [48] O. Kahn, *Molecular Magnetism*, VCH Publishers, Berlin, 1993.
- [49] S. Hill, R.S. Edwards, N. Aliaga-Alcalde, G. Christou, *Science* 302 (2003) 1015.
- [50] D. Gatteschi, R. Sessoli, *Angew. Chem., Intl. Ed.* 42 (2003) 268.
- [51] A.V. Pali, S.M. Ostrovsky, S.I. Klokishner, B.S. Tsukerblat, C.P. Berlinguette, K. Dunbar, J.R. Gálan-Mascarós, *J. Am. Chem. Soc.* 126 (2004) 16860.
- [52] J.B. Goodenough, *Magnetism and the Chemical Bond*, Wiley and Sons, New York, 1963.
- [53] P.W. Anderson, in: F. Seitz, D. Turnbull (Eds.), *Solid State Physics*, New York, 1963.
- [54] J. Glerup, D.J. Hodgson, E. Pedersen, *Acta Chem. Scand., Ser. A* 37 (1983) 161.
- [55] H. Weihe, H.U. Güdel, H. Toftlund, *Inorg. Chem.* 39 (2000) 1351.
- [56] S.W. Gordon-Wylie, E.L. Bominaar, T.J. Collins, J.M. Workman, B.L. Claus, R.E. Patterson, S.A. Williams, B.J. Conklin, G.T. Yee, S.T. Weintraub, *Chem. Eur. J.* 1 (1995) 528.
- [57] G. Blondin, J.-J. Girerd, *Chem. Rev.* 90 (1990) 1359.
- [58] A. Stubna, D.H. Jo, M. Costas, W.W. Brennessel, H.P. Andres, E.L. Bominaar, E. Münck, L. Que, *Inorg. Chem.* 43 (2004) 3067.
- [59] S.W. Gordon-Wylie, W.B. Blanton, B.L. Claus, C.P. Horwitz, T.J. Collins, C. Boskovic, G. Christou, *Inorg. Synth.* 33 (2002) 1.
- [60] S. Mukherjee, T. Weyhermüller, E. Bothe, K. Wieghardt, P. Chaudhuri, *Dalton Trans.* 22 (2004) 3842.
- [61] D.S. Marlin, E. Bill, T. Weyhermüller, E. Bothe, K. Wieghardt, *J. Am. Chem. Soc.* 127 (2005) 6095.
- [62] A.K. Patra, E. Bill, T. Weyhermüller, K. Stobie, Z. Bell, M.D. Ward, J.A. McCleverty, K. Wieghardt, *Inorg. Chem.* 45 (2006) 6541.
- [63] T.J. Collins, K.L. Kostka, E. Münck, E.S. Uffelman, *J. Am. Chem. Soc.* 112 (1990) 5637.